DOE/NASA/0131-2
NASA CR-168278

Numerical Modeling of Turbulent Flow in a Channel

Y.-W. Dai, A. F. Ghoniem,
F. S. Sherman, and A. K. Oppenheim
University of California

March 1983

Prepared for
NATIONAL AERONAUTICS AND SPACE ADMINISTRATION
Lewis Research Center
Under Grant NAG 3-131

DEPARTMENT OF ENERGY
Office of Basic Engineering Research
Under Contract W-7405-ENG-48

and

NATIONAL SCIENCE FOUNDATION
Under Grant CPE-8115163

DISCLAIMER

DOE/NASA/0131-2
NASA CR-168278

Numerical Modeling of Turbulent Flow in a Channel

Y.-W. Dai, A. F. Ghoniem,
F. S. Sherman, and A. K. Oppenheim
University of California
Berkeley, California

March 1983

Prepared for
National Aeronautics and Space Administration
Lewis Research Center
Cleveland, Ohio 44135
Under Grant NAG 3-131

Department of Energy
Office of Basic Engineering Research
Under Contract W-7405-ENG-48

and

National Science Foundation
Under Grant CPE-8115163

CONTENTS

NOMENCLATURE

A	area
B	normalized inlet height of channel
d_j	influence factor of a vortex sheet
F	differential transformation function
G	the Green's function
h	length of a vortex sheet
H	height of channel
HT	height of step
i	imaginary unit of complex number, $\sqrt{-1}$
J	number of vortex blobs
p	normalized pressure, by ρu_∞^2
$\underline{r}$	(x,y) position vector
r_o	cutoff radius
R	Reynolds number
t	nondimensional time
T	numerical time steps
$\underline{u}$	(u,v) normalized velocity vector, by u_∞
u	streamwise component of velocity
v	transverse component of velocity
W	conjugate complex velocity, $u - iv$
x,y	Cartesian space coordinate
z	complex coordinate in physical plane, $x + iy$
α	expansion ratio, $H/(H-Ht)$
γ	circulation per unit length, $\int \xi dy$
Γ	circulation, $\int \xi dA$
δ	Dirac delta function or boundary layer thickness
δ_s	thickness of numerical sheet layer
ζ	complex coordinate in transformed plane
η	Gaussian random variable
μ	viscosity
ξ	vorticity
ρ	density
σ	standard deviation, $\sqrt{2\ k/R}$
ϕ	velocity potential
ψ	stream function

∇ gradient operator

∇^2 Laplacian operator

SUBSCRIPTS:

f in free stream

i index

j vortex element

r at reattachment point

o at cutoff radius

+ at right edge of a grid

- at left edge of a grid

$\_$ vector

∞ at inlet

SUPERSCRIPTS:

' fluctuation part

$\overline{}$ average value

~ complex conjugate

CHAPTER 1

INTRODUCTION

The reattachment of a turbulent shear layer is an important process in a large number of practical engineering configurations such as diffusers, airfoils, and combustors. In order to predict these complicated flows, we must understand and be able to predict the behavior of reattaching shear layers. However, our current understanding of reattachment is very limited.

Among two-dimensional reattaching flows, the one-sided backward-facing step flow has the simplest geometry. The separating line is straight and fixed at the edge of the step, and there is only one separated zone. Even so, the flow field is still very complex, as illustrated in figure 1.1. A boundary layer separates from the step edge, becoming a free shear layer. The separated shear layer grows into a recirculating flow. The shear layer curves sharply downwards in the reattachment zone and impinges onto the wall. Within the reattachment zone, the shear layer is subjected to the effects of strong curvature, an adverse pressure gradient, and strong interaction with the wall. Part of the shear layer fluid is deflected upstream into the recirculating flow to supply the entrainment. The length of the separation bubble fluctuates in an apparently random manner. Just because of its simple geometry and its typical and complex fluid mechanics, a great deal of attention has been directed to it in past years, both numerically and experimentally.

Hsu (1950) was the first to measure mean flow and turbulence profiles in a low-speed flow behind a large step. He noted little unsteadiness in the position of reattachment. Another early study is that of Abbott and Kline (1961), who measured mean velocity profiles for both single and double steps of various heights. They used water flow with flow-visualization techniques, and observed that the flow near reattachment was very unsteady. Kim, et al. (1978), measured mean velocity, Reynolds stresses, and intermittency in a sudden-expansion channel flow using hot-wire anemometers. Eaton and Johnston (1980) measured the reattachment length velocity and turbulence profiles. They also studied the effect of the initial boundary layer state and step height and spanwise vortex structure. Comparison was made with the plane-mixing layer. Their measurements provide well-documented data for the backward-facing step flow.

Some new views of the structure of these turbulent flows have been expressed. Laufer (1975) concluded that "these turbulent flows are not as chaotic as has been previously assumed, and there is some order in their motion with an observable chain of events reoccurring randomly with a statistically definable mean period," "eddies have a characteristic shape, size, and convective motion that can be determined with a relatively small standard deviation." Roshko (1976) suggested that with every shear flow is associated an identifiable, characteristic structure, and the development of the flow is controlled by the interactions of these structures: large eddies are formed in a quasi-orderly fashion, carried through the mixing layer, and grow through coalescence and engulfment. Ganji and Sawyer (1979) concluded that "large-scale coherent structures are observed to dominate the shear layer behind a backward-facing step as well as other free shear layers."

A comprehensive review of the research of backward-facing step flow is given by Eaton and Johnston (1980).

Numerical analysis of turbulent flow is traditionally based on a finite difference treatment of appropriately averaged Navier-Stokes equations, combined with some correlations of turbulent fluctuations, the so-called closure model. Recently Taylor, et al. (1981), obtained a numerical solution using the finite-element method and a two-equation model of turbulence. In these methods an average behavior of the flow field is obtained in Eulerian description. These methods are powerful instruments in many engineering applications.

However these methods have some shortcomings. Of these, Ghoniem, et al. (1980), indicated that the averaging process deprives the equations of essential information about the mechanism of turbulence, that the turbulence model required for the closure relations has to be postulated and adjusted to match the experimental data, and that these techniques introduce numerical diffusion which tends to smooth out local perturbations, an effect which is especially harmful at high Reynolds numbers.

All these points are overcome by the Random Vortex method developed by Chorin (1973). This method is intended for the approximation of flows at high Reynolds numbers. The main features, as indicated by Chorin (1980), are as follows: (1) the nonlinear terms in the Navier-Stokes equation are taken into account by a detailed analysis of the inviscid interactions between vortices of small but finite cores ("vortex blobs"); (2) viscous diffusion is taken into account by adding to the motion of the vortices a small random Gaussian

component of appropriate variance; and (3) no-slip conditions are approximated by a vorticity-creation algorithm.

Partial convergence proofs for the Random Vortex method are given by Chorin, et al. (1980), and Hald (1979).

The RVM is a grid-free method. It provides a Lagrangian description of the vorticity distribution of the flow field, which is especially useful in investigating the large-scale turbulence structures and has already been successfully applied to many turbulent shear layer flows in recent years, as reviewed by Leonard (1980) and Sod (1980).

An outline of RVM is presented in Chapter 2. The numerical computation was based on the pioneer work of Ghoniem, Chorin, and Oppenheim (1980) in which the vorticity field was computed for a step height of 1/2.

The objectives of this work were to model numerically the turbulent flow in a two-dimensional channel with other step heights by the Random Vortex method, to investigate the reattachment process and the behavior of the large-scale eddies in the flow, and to study both the time-variable and the time-mean properties and the effects on the state of the incoming flow, the step height on the reattachment process, and the flow structures.

CHAPTER 2

FORMULATION AND COMPUTATION

2.1 FORMULATION

The problem we treat is formulated on the basis of the following idealizations:

(1). The flow is two-dimensional;

(2). The flowing substance is incompressible; and

(3). The inlet velocity is uniform.

The normalized governing equations are as follows:

Continuity equation $$\underline{\nabla} \cdot \underline{u} = 0 \tag{1}$$

Navier-Stokes equation $$\frac{D\underline{u}}{Dt} = R^{-1}\nabla^2 u - \underline{\nabla} P \tag{2}$$

where $\underline{u}(\underline{r}) = (u,v)$ is the velocity vector normalized by the inlet velocity u^{∞}, $\underline{r}$ is the position vector normalized by H, t is the time normalized by H/u_{∞}, H is the reference length - channel height, R is the Reynolds number of inlet flow, and p is the pressure normalized by ρu_{∞} where ρ denotes the reference density of the media, and while

$$\frac{D}{Dt} = \frac{\partial}{\partial t} + \underline{u} \cdot \underline{\nabla}$$

is the material derivative, ∇^2 is the Laplacian operator, and $\underline{\nabla}$ is the usual del operator.

Vorticity is given by

$$\underline{\xi} = \underline{\nabla} \times \underline{u} \tag{3}$$

Taking the curl of the Navier-Stokes equation, we have the so-called vortex transport equation:

$$\frac{D\underline{\xi}}{Dt} = R^{-1}\nabla^2\underline{\xi} \tag{4}$$

while

$$\nabla \times \nabla P = 0$$

Thus the flow is described by equations (1), (3), and (4). Equations (1) and (3) are used to determine the velocity field $\underline{u}(x,y)$, and (4) is employed to update the vorticity field $\underline{\xi}(x,y)$. In a two-dimensional domain, $\underline{\xi}$ has one nonzero component only.

The boundary condition along all solid boundaries is

$\underline{u} = 0$ (5)

and at the inlet is

$\underline{u} = (1,0)$ (6)

The boundary condition at the inlet of the channel is specified by a uniform stream that is generated by a source of potential flow located at infinity to the left side of the step. The vorticity intensity of the inlet flow is assumed zero in all the computations presented here.

For the boundary condition on the right side of the channel, theoretically, the fully developed turbulent channel flow is reached at infinity. However, in numerical calculation, only a certain finite length of the channel is considered. For simplicity, the vorticity intensity beyond the length of consideration is also assumed zero. The reasons which allow us to do so are:

(1). The flow beyond the reattachment point approaches normal channel flow downstream, which is symmetric about the channel axis. Thus the effects of the vorticity field far downstream on the flow field under consideration almost cancel each other.

(2). The interest of this research is mostly concentrated on the reattaching shear flow, which starts from the separation point and extends less than 10 step heights downstream.

Additionally, the longer the length of channel to be considered, the more vortex elements are involved, and the more computer time is needed. Thus, in the numerical computation, the length of the channel has been chosen about two to three times the reattachment length.

2.2 VORTEX DYNAMICS

2.2.1 Vortex Blobs

Consider the inviscid fluid flow first. The vorticity field $\underline{\xi}$ produces a field $\underline{u}$ which transports it in turn. The flow field can be expressed in term of vortices, i.e., point vortices in a two-dimensional domain which can be described as

$\xi_j = \Gamma_j \delta(z - z_j)$ (7)

where Γ_j is the circulation of the vortex at Z_j, δ is the Dirac delta function, and Z_j is the complex coordinate of vortex ξ_j.

Define the complex velocity potential as

$W = \phi + i\,\psi$ (8)

where ϕ is the velocity potential and ψ is the stream function. According to the potential flow theory (Milne-Thomson (1976)), the conjugate complex velocity can be solved as

$$U = u - iv = \frac{dW}{dZ} \tag{9}$$

Suppose that the entire flow field consists of a set of point vortices with complex potentials $W_1, \ldots\ldots W_n$ respectively, where

$$W_j = -\frac{i\Gamma_j}{2\pi} \mathrm{Ln}\ (Z - Z_j) \tag{10}$$

Thus the velocity field is given by

$$\frac{dW}{dZ} = \frac{d\sum W_j}{dZ} \tag{11}$$

according to the superposition principle.

This is the classical point vortex method. Now consider the structure of a point vortex. From equations (9) and (10), one obtains

$$U = \frac{dW_j}{dZ} = -\frac{i\Gamma_j}{2\pi(Z - Z_j)} \tag{12}$$

The modulus of the induced velocity approaches zero at a far distance. However as Z approaches Z_j, the center of the vortex, the modulus of the induced velocity approaches infinity which is physically unrealistic due to viscosity of the fluid. Mathematically the center of the vortex is a singular point. To remove this singularity Chorin (1973) introduced the cutoff radius r_o, i.e., radius of the core of vortex within which the modulus of induced velocity $|U|$ keeps constant

$$U_j = -\frac{i\Gamma_j\ |Z - Z_j|}{2\pi(Z - Z_j)\ \mathrm{Max}\ (|Z - Z_j|,\ r_o)} \tag{13}$$

The vortex element with such a treatment is called a vortex blob.

2.2.2 Conformal Transformation

The above mentioned discrete vortex method applied originally only to an infinite domain without boundary. To satisfy exactly the normal boundary condition at the wall, given by equation (5), the method of images was used. The Schwartz-Christoffel transformation was used to map the flow field from the physical Z plane onto the upper half ζ plane, shown in figure 2.1. The solid wall of the channel was transformed to the horizontal axis in the ζ

plane correspondingly. The theorem of Schwartz-Christoffel (Milne-Thomson (1976)) is

$$\frac{dZ}{d\zeta} = K(\zeta - a)^{\frac{\alpha}{\pi}-1} (\zeta - b)^{\frac{\beta}{\chi}-1} (\zeta - c)^{\frac{\gamma}{\pi}-1} \quad \ldots\ldots \tag{14}$$

For a backward-facing step channel we have

$$\frac{dZ}{d\zeta} = K^{-1} (\zeta - a)^{\frac{1}{2}} (\zeta - b)^{-\frac{1}{2}} = \frac{H}{H\zeta} \frac{\zeta - b}{\zeta - a} \tag{15}$$

where H is the channel height, and a and b are the coordinates in the ζ plane corresponding to points D and E in figure 2.1, respectively. If particularly, we choose $a = 1$, $b = \alpha^2$, $\alpha = 1/B$, where B is the inlet height of channel, we have thus

$$\frac{dZ}{d\zeta} = \frac{1}{\pi\zeta} \frac{\zeta - 1}{\zeta - \alpha^2} \tag{16}$$

Furthermore we can solve Z on the wall from ζ by the method of integration with a parameter:

$$Z = \frac{1}{\pi} \left[\mathrm{Ln} \frac{1 + t}{1 - t} - \frac{1}{\alpha} \mathrm{Ln} \frac{\alpha + t}{\alpha - t}\right], \text{ where } t = \frac{\alpha^2 - \zeta}{1 - \zeta} \tag{17}$$

But there is no explicit expression for ζ from Z, except in case of $B = 1/2$, i.e., $\alpha = 2$, as done by Ghoniem, et al. (1980). Thus here we use the Runge-Kutta method to find $\zeta(Z)$ from the reciprocal relation of equation (16):

$$\frac{d\zeta}{dZ} = \pi\zeta \frac{\zeta - \alpha^2}{\zeta - 1} \tag{18}$$

Since we check the no-slip condition (section 2.2.4) at a set of points, h apart from each other, regularly arranged along the wall in the physical Z plane, we must find the coordinates of the set of points in the ζ plane, corresponding to the regularly arranged wall points in the Z plane. We know from the conformal transformation theory that the wall of the channel is transformed to the horizontal axis in the ζ plane. To use the numerical mapping technique we must have a couple of reference points (ζ_o, Z_o) as the starting point in numerical integration. The coordinates of wall points in the Z plane are predetermined, but unfortunately we do not have an explicit expression for $\zeta(Z)$ except when $HT = 1/2$. Thus here we first pick a point on the horizontal axis in the ζ plane by experience, then use the trial-and-error method to find the reference point in the ζ plane which is sufficiently close to the point corresponding to the first of the regularly

arranged wall points in the Z plane for the numerical mapping technique in order to get accurate results. Since the Schwartz-Christoffel transformation in the current case is strongly nonlinear, especially as ζ approaches zero, α^2 or one, where $d\zeta/dZ$ approaches zero or infinity respectively, such a trial-and-error method sometimes might be time-consuming. Fortunately the wall points mapping, as well as the spatial grid points mapping, in the Eulerian description has to be done only once for each geometry. To obtain accurate numerical transformations, double precision is used, and transformed data are checked by remapping back to the Z plane using the explicit expression $\zeta \rightarrow t \rightarrow Z$. Also the numerical results for the transformation of wall points are checked with the analytic results in a particular case of step height 1/2, which was done by Ghoniem, et al. (1980). The numerical mapping error in the position vector is found to be less than 1×10^{-6}.

As shown in figure 2.1, the channel was transformed to the upper half ζ plane. The boundary was transformed to the horizontal axis in the ζ plane, and the uniform inlet flow in the physical Z plane becomes a half source flow in the ζ plane at the origin. To satisfy the normal boundary condition as specified by equation (5), we introduce the image system of the original source and vortex terms. The corresponding complex velocity field $U(\zeta)$ in the ζ plane produced by the source and vortices and their images about the horizontal axis is given by

$$U(\zeta) = \frac{dW_S(\zeta)}{d\zeta} + \sum \frac{dW(\zeta, \zeta_j)}{d\zeta} \sum \frac{dW(\zeta, \tilde{\zeta}_j)}{d\zeta} \tag{19}$$

where $W_S(\zeta)$ is the complex velocity potential of the source, $W(\zeta, \zeta_j)$ is the complex velocity potential of a vortex with the center at ζ_j, and $\tilde{\zeta}_j$ is the complex conjugate of ζ_j. To find the velocity distribution in the physical Z plane, the inverse transformation is simply employed.

2.2.3 Random Walk Simulation

The unsteady vorticity distribution is governed by equation (4), the vorticity transport equation. The operator can be split into two parts:

Convective part $$\left(\frac{\partial \xi}{\partial t}\right)_c = - \underline{u} \cdot \underline{\nabla}\, \underline{\xi} \tag{20}$$

Diffusive part $$\left(\frac{\partial \xi}{\partial t}\right)_d = R^{-1} \nabla^2 \underline{\xi} \tag{21}$$

According to the convection operator, the vortex blobs move at the local velocity. For the diffusion part, it is well known mathematically that the solution of the one-dimensional diffusion equation with a Dirac delta function as the initial condition is the Green's function

$$G(x,t) = \frac{R}{4\pi t}^{\frac{1}{2}} \exp - \frac{Rx^2}{4t} \tag{22}$$

This is also the probability density function of a Gaussian random variable with zero mean and a standard deviation $\sigma = (2t/R)^{1/2}$. Thus Chorin (1973) introduced a scheme of adding a random walk each time step to simulate the diffusion effect. Two-dimensional diffusion was treated independently. Thus the new locations of each vortex element after a time step are given approximately by

$$Z_j(t + \Delta t) = Z_j(t) + \tilde{U}(Z_j)\,\Delta t + \eta_j \tag{23}$$

where $Z_j(t)$ is the old location of the vortex element, $\tilde{U} = u + iv$ is the local velocity in complex form, and $\eta_j = \eta_x + i\eta_y$ is the two-dimensional random walk in that time interval.

2.2.4 Vortex Creation

To satisfy the no-slip boundary condition, the velocities are calculated at a set of regularly arranged points h apart from each other along the wall as mentioned above. Wherever the tangential velocity is not zero, a vortex with a circulation of $u_w h$ is created and incorporated into the computation of the next time step.

2.2.5 Vortex Sheets

In the boundary layer region the vortex blobs do not provide a good description, since one cannot use very tiny vortex blobs to fill up the boundary layer to achieve good precision. Otherwise it would be very time-consuming.

From the boundary layer assumption

$$\frac{\partial^2 u}{\partial x^2} << \frac{\partial^2 u}{\partial y^2} \tag{24}$$

$$\frac{\partial v}{\partial x} << \frac{\partial u}{\partial y} \tag{25}$$

Chorin (1973) proposed the use of vortex sheets, which are elongated in the tangent direction, to represent the vorticity very near the wall, where a good evaluation of the vorticity is given by the simple expression

$$\zeta = - \partial u/\partial y \tag{26}$$

The tangential component of velocity u can then be found by integration of equation (26), and the normal component of velocity v can be found with the use of continuity equation (1). Ghoniem, et al. (1980), gives a detailed numerical treatment.

The motion of the vortex sheets is simulated similarly by the convective and diffusive (random walk) effects, but with $n_j = 0 + i n_y$ in accordance with the boundary layer diffusion approximation.

2.3 ALGORITHM

The computations are performed as follows:

First, the value of h, the sheet length specifying the spatial resolution, is chosen properly. The value of the time interval Δ is then fixed in accordance with the stability condition (Chorin (1980)):

$$\Delta t \leq h/\text{Max } (\underline{u}) \tag{27}$$

For a given Reynolds number, this specifies the standard deviation σ. The thickness of the wall layer, within which vorticity is represented by sheets, is then taken as a multiple of σ.

At time zero only the incoming potential flow associated with the source in the ζ plane exists. Vortices are created by the no-slip condition at numerically specified points along the wall. The displacement of the vortex sheet accounts for the combined effects of convection and diffusion. Whenever a vortex sheet moves outside the sheet layer, it becomes a vortex blob and vice versa.

Once the position and the strength of both the vortex sheets and blobs are established, the flow field at a given time step is fully determined. The vortex blobs appear only as a consequence of the displacement of vortex sheets outside the wall layer.

The blobs' ability to induce strong motion normal to the wall is an essential computational feature which allows the scheme to simulate hydrodynamic instability and represent a two-dimensional version of turbulent flow.

The immediate product of the calculation is a Lagrangian description of the flow, specifically a list of the current positions of all the vortex elements. An Eulerian description of the velocity for prescribed points of observation can be calculated from the Lagrangian data. Statistical properties of the Eulerian data are then evaluated (as will be described in detail in Chapter 3) to allow comparison with laboratory measurements.

2.4 VELOCITY AND TURBULENCE PROFILES

The definition of turbulent flow given by J. Hinze is that "turbulent fluid motion is an irregular condition of flow in which the various quantities show a random variation with time and space coordinates, so that statistically distant average values can be discerned." The momentary value of the velocity is written as

$$u = \bar{u} + u' \tag{28}$$

where the overscore denotes the average value, and u' is the fluctuation of the velocity component. The intensity of the turbulence fluctuations is defined as the root-mean-square value $\overline{u'^2}$. The relative intensity is then defined by the ratio $\overline{u'^2}/\bar{u}$. Also, the so-called apparent or Reynolds stress is defined as $-\rho\,\overline{u'v'}$, and the relative Reynolds stress as $-\rho\,\overline{u'v'}/\bar{u}^2$. These velocity and turbulence profiles are calculated over some time interval of quasi-steady turbulent flow in Eulerian description in which the numerical transformation is used for the Eulerian grid mapping.

In the presentation of results all velocities are normalized by the speed of the uniform inlet flow.

CHAPTER 3

RESULTS AND DISCUSSION

The computations were performed at $Re = 10^4$ for step heights of 1/3, 1/4, and 1/5 (i.e., at expansion ratios 3/2, 4/3, and 5/4, respectively) and at $Re = 10^5$ for step height 1/3 to model the process recorded photographically by Ganji and Sawyer (1979) and to investigate the effects of step height and the Reynolds number. Computation for step height 1/5 was performed on a CDC 7600 computer and the others were carried out on a VAX computer.

Sequential pictures of flow development in the Lagrangian description were plotted for each flow condition showing the vortex distribution and the large-scale structures.

The length of reattachment was traced for each flow condition to show the development and fluctuation of the recirculation zone.

The velocity distribution in the Eulerian mesh is calculated at each time step in certain time intervals for averaging. Also, the streamwise velocity component is calculated at six typical locations taken from the recirculation zone, reattachment zone, and the channel turbulent flow rebuilding region at every 10 time steps from the very beginning. This is plotted in figure 3.29 (a to c), and the result is time-dependent.

The local variation with time of the velocity distribution in the Eulerian description may attribute to the following separately recognizable phenomena:

(1). The uniform flow is imposed at the inlet and requires some time to adjust the flow to the fully developed turbulent flow. Numerically, this process is very time-consuming.

(2). To model turbulent flow, the computation employs discrete elements of vorticity which cause relatively large fluctuations of velocity at an observing point whenever they pass close by that point. The displacement of each vortex element during each time step is partially random (the diffusion part of displacement). The discretization and the random components of displacement contribute some artificial unsteadiness.

3.1 UPSTREAM CONDITIONS

The state of the entry flow can have a substantial effect on the behavior of the shear layer. The condition of the boundary layer at separation can

affect the shear layer's virtual origin, initial breakdown, growth rate, reattachment point, and turbulence development (Bradshaw (1966) and Eaton and Johnston (1980)). The major scaling parameters assessing the state of the boundary layer are the momentum thickness and the boundary layer thickness, which in turn are controlled by the Reynolds number of the entry flow and the inlet length. In this work, uniform inlet flow was assumed for convenience, and the normalized inlet length, 1.0, was chosen in most cases to establish the boundary layer with a certain thickness at the separation point, as well as to save computer time.

3.2 MEAN VELOCITY PROFILES

The region downstream from the step can be divided into three zones:

(1). A recirculation zone,

(2). A reattachment zone, and

(3). A developing boundary layer zone.

The recirculation zone is characterized by strong negative velocities below the step and ends with the reattachment point where the flow almost ceases to circulate, and positive streamwise velocity profiles fill out the entire section of the channel thereafter. A boundary layer starts to grow after reattachment and the fluid flow turns into a developing flow in a channel.

The velocity distributions along channels of step heights 1/3, 1/4, and 1/5 at $Re = 10^4$ and step height 1/3 at $Re = 10^5$ are shown in figures 3.1, 3.2, 3.3, and 3.4, respectively. Values of streamwise velocity of numerical and experimental data (Kim, et al. (1978)) are plotted for the case of step height 1/3 and $Re = 10^4$. The results seem to be in good agreement near the step where the numerical solution has almost reached a stationary state, while the disagreement is more pronounced downstream where the flow is still under development. The change in the calculated velocity profiles with time is shown in figure 3.28 in which the top figure is calculated after 158 time steps, while the bottom figure is calculated after 291 time steps. A typical maximum value of reverse velocity calculated in the recirculation zone is about 0.4 to 0.5 U_f, while the experimental value reported by them is about 0.25 U_f where U_f is the free stream velocity which corresponds to the mass average velocity in the downstream channel in the numerical calculation.

Beyond the reattachment point, the flow field approaches the turbulent flow in a channel with parallel walls. The transverse component of velocity fluctuates around zero, while the streamwise velocity profiles develop slowly into a symmetric distribution around the center line of the channel. According to Bradshaw and Wang (1972), it will take about 50 step heights downstream for the flow to relax to the normal internal turbulent flow.

The upper edge of the recirculation zone is fairly straight until $X/X_r = 0.6$ where X_r is the reattachment length; it then drops down toward the bottom wall.

The mean velocity profiles of the boundary layer at three typical locations on the bottom wall selected from the recirculation region, the reattachment region, and the boundary layer rebuilding region after reattaching are shown in figures 3.5 to 3.10 for the case of step heights 1/3 and 1/4. Figure 3.11 shows the corresponding experimental profiles in the case of step height 1/3. In general, both results show the same trend of variation.

An important parameter in turbulent flow over a backward facing step is the reattachment length. The reattachment point R is defined as a point where the dividing stream line returns to the wall. A sketch for a reattaching shear layer behind a step with a definition of the reattachment length is shown in figure 3.12.

The reattachment length is controlled to a large extent by the step height which affects the growth of the shear layer into the recirculation zone.

The lower edge of the shear layer is difficult to locate due to the very gradual decrease in the slope, while the reattachment length can be easily estimated from the streamwise velocity distribution. Values of the estimated reattachment length from the mean velocity distribution in the neighborhood of the bottom wall are 2.2 and 1.8 for $Re = 10^4$ and step heights 1/3 and 1/4 respectively, and 1.9 for $Re = 10^5$ and step height 1/3. The values of reattachment length normalized by step height are 6.7, 7.2, and 5.8, respectively. From the transient velocity distribution at each numerical time step we can also assess the development of the recirculation zone shown in figures 3.13 to 3.16. The reattachment length increases monotonically in the first stage, then wanders upward and fluctuates around some average value when the flow approaches the quasi-stationary state due to the splitting and coalescence mechanism of large-scale eddies. The value of the reattachment length estimated from the mean velocity distribution coincides with the asymptotic value of that deduced from the transient velocity distribution. The computed

normalized reattachment length at Re = 10^4 is in good agreement with the experiment value X/X = 7 + 1 from Kim, et al. (1978). The numerical data at step height 1/3 with different Reynolds numbers (table 3.1) are consistent with the results of Eaton and Johnston (1980), who concluded that the value of reattachment length is maximum at a medium Reynolds number, then decreases to approach an asymptotic value with increasing Reynolds numbers.

3.3 MEAN TURBULENCE PROFILES

The turbulence intensity and Reynolds stress profiles are shown in figures 3.17 to 3.19 for step heights 1/3 and 1/4, respectively. The region of the relatively high turbulence level is around the dividing stream line between the separation point and the reattachment point. Approaching the reattachment zone, the turbulence level decreases slightly. Beyond the reattachment point, the turbulence profiles begin to take on the characteristics of the normal turbulent channel flow where the turbulence level is almost uniform in the turbulent core flow region. These general trends are also observed in the experimental results such as Kim, et al. (1978), Eaton and Johnston (1980), and Etheridge and Kemp (1978).

The positions of maximum turbulence intensity are shown in figures 3.20 and 3.21 for step height 1/3 with Reynolds numbers 10^4 and 10^5 respectively, and compared with Eaton and Johnston (1980). The qualitative trends agree. The vertical locations of maximum turbulence intensity initially (from separation point) coincide with the step level (Y/HT = 1). It then dips slightly toward the recirculation zone and rises back toward the center line after reattachment.

The turbulence intensity in streamwise direction reaches a maximum in the vicinity of the wall. However on the wall it goes back to zero. It should be mentioned here that the wall boundary layer is very thin and the details of the turbulence profile inside it are not shown on the graph.

3.4 LARGE-SCALE TURBULENCE STRUCTURE

The presence of large-scale structures in the plane-mixing shear layer and in the reattaching shear layer has been experimentally established by Brown and Roshko (1974), Eaton and Johnston (1980), and Ganji and Sawyer (1979) and is shown in numerical results by Ashurst (1979) and Ghoniem, et al. (1980).

The large-scale structures form early in the shear layer from a Kelvin-Helmholtz instability (Sherman (1976)). The structures are basically two-dimensional and grow by pairing and entrainment as they move downstream. Eaton and Johnston (1980) showed that the large eddy length scale was significantly longer in the spanwise direction than in the cross-streamwise direction and that pairing was an important growth mechanism of the shear layer. They also indicated evidence that the large-scale structure is occurring even in the high Reynolds number case. High speed schlieren photographs in Ganji and Sawyer (1979) show that large-scale structures are prominent throughout the flow field.

The sequence of pictures of the flow filed in terms of the distribution of vorticity taken from computer-generated movies for step heights 1/5, 1/4, 1/3 and Re = 10^4, and step height 1/3 and Re = 10^5 is shown in figures 3.22 to 3.25 respectively, where the dot denotes the center of each discrete vortex to which a short segment is attached and stands for the velocity vector for that vortex.

Figure 3.22 shows a typical development of the vorticity field from the beginning. The flow is impulsively started by applying the uniform velocity at the inlet section of the channel. Vortices are created along the solid walls to satisfy the no-slip condition and are introduced into the flow as vortex sheets. Whenever the vortex diffuses outside the sheet layer, it becomes a vortex blob and is plotted. All the vortices are introduced along the wall and stay there until they diffuse into the field.

A separated shear layer is formed by separation of the boundary layer on the step and grows while traveling downstream. The vortices concentrated beyond the separation point construct gradually the large-scale structures. They grow while convecting downstream, elongate, and split, as shown from T = 4.00 to T = 6.00, for example, then break down into eddies with a relatively small scale around the reattachment zone. A boundary layer starts to form after reattachment and the fluid flow turns into a developing flow in a channel.

What happens to the large structures in the approaching shear layer at reattachment is not yet clear. Bradshaw and Wang (1972) suggested that the large structures are torn roughly in two somewhere near the reattachment zone. Chandrsuda (1975) suggested another possibility that the large structures move alternately downstream and upstream. Kim, et al. (1978), believe that the splitting of a large structure is not the only phenomenon which takes place at

reattachment. Eaton and Johnston (1980) observed through a crude flow-visualization experiment that large structures passed through the reattachment zone and never swept upstream. In this study, the sequential pictures of the numerical flow field plots show that no large structure is swept upstream. The results seem to support the postulate of a splitting mechanism for large structures around the reattachment zone.

Figure 3.26 shows the comparison of flow development at step height 1/3 with different Reynolds numbers. It is found that the large-scale structures in high Reynolds number cases are confined in a relatively short distance from the separation point. This results in a relatively short reattachment length as plotted in figures 3.13 and 3.16, which is consistent with the experimental results of Eaton and Johnston (1980).

By comparing the flow pictures of different step heights at the same Reynolds number it is found that the scales of large structures are controlled by the step height, which corresponds to the variation of reattachment length with step height.

Figure 3.27 and table 3.2 compare the flow development with different inlet lengths, hence with different boundary layer thicknesses at the separation point. The large-scale structure appears earlier from the well-developed boundary layer at separation point in the longer inlet length case.

3.5 SUGGESTIONS FOR FUTURE WORK

As said above, the Random Vortex is indeed a very useful method for investigating the large-scale structure of turbulent flows. The results obtained here are really very encouraging, but there are some evidences showing that the flow did not reach the quasi-steady state. The reattachment length seems to continue to increase. Figure 3.28 shows the average velocity profiles of step height 1/3 and Re = 10^4 in different time intervals: it is seen that the flow field is still developing. Also from figure 3.29 (a to c), it is seen that the standard deviation at points closer to the bottom wall is larger than that at points along the step level. The standard deviation decreases downstream and the value of the streamwise velocity still oscillates widely. Consequently, further computation is probably advisable.

On the other hand, further computation is time-consuming. Since the velocity field induced by each vortex blob reaches everywhere in the flow

field, we must account for all the vortices to obtain the velocity distributions. Thus the total computer time needed to find the vorticity and velocity distributions at time step is approximately in proportion to N^2, where N is the number of vortex blobs at that time step. In the VAX computer the CPU time for a single time step is about 20 minutes at 2000 vortex blobs and 45 minutes at 3000 vortex blobs. A typical magnitude of vortex blobs at time step 200 is 2000, and 3000 at time step 350. It seems that a more powerful computer is needed.

For calculating the averaging profiles in the Eulerian description, the averaging time period is picked from one quasi-cycle as seen from the movie picture series plotted by the computer. It is found roughly that a quasi-cycle consists of about 50 to 80 time steps from the movies as well as from figures of $u(t)$. Better averaging profiles might be expected if more than one quasi-cycle were covered. This would also suggest the use of a computer with faster computing speed as well as more data storage.

CHAPTER 4

CONCLUSIONS

The main objectives of this work, as stated in the Introduction, were to model numerically the turbulent flow in a two-dimensional channel with variable step height by the Random Vortex method and to investigate both time-variable and time-average behaviors of the flow.

Conclusions from these numerical results and a comparison with available experimental results are:

(1). RVM is capable of modeling the essential features of the reattaching turbulent internal flow as observed by Schlieren visualization.

(2). The numerical results support the existence of the large-scale structure in the reattaching turbulent internal flow and provide a clarification of the essential process of the formation, growth, splitting, and propagation of the large-scale structures.

(3). The numerical calculated reattachment lengths are in good agreement with the experimental results.

(4). The numerical calculated velocity profiles are qualitatively consistent with the experimental data.

REFERENCES

Abbott, D. E. and S. J. Kline (1962), "Experimental Investigation of Subsonic Turbulent Flow over Single and Double Backward Facing Steps," Trans. ASME, J. Basic Engineering, vol. 84D, Series D, 1962, pp. 317-325.

Ashurst, W. T. (1979), "Numerical Simulation of Turbulent Mixing Layer via Vortex Dynamics," "Proc. of the First Symposium on Turbulent Shear flows," pp. 402-413.

Batchelor, G. K. (1967), "An Introduction to the Fluid Mechanics" Cambridge Univ. Press, London.

Bradshaw, P. (1966), "The Effect of Initial Conditions on the Development of Free Shear Layer," J. Fluid Mechanics, 26 pp. 225-236.

Bradshaw, P. and F. Y. F. Wang (1972), "The Reattachment and Relaxation of a Turbulent Shear Layer," J. Fluid Mech., 52, part 1, pp. 113-135.

Brown, G. L. and A. Roshko (1974), "On Density Effects and Large Structure in Turbulent Mixing Layers," J. Fluid Mech., 64, pp. 775-816.

Chandrsuda, C. (1975), "A Reattaching Turbulent Shear Layer in Incompressible Flow," Ph.D Thesis, Imperial College of Science and Technology.

Chorin, A. J. (1973), "Vortex Sheet Approximation of Boundary Layers," J. Comp. Phys. 27, 428-442.

Chorin, A. J. (1973), "Numerical Studies of Slightly Viscous Flow," J. Fluid Mec., 57, 785-796.

Chorin, A. J. and Marsden, J. E. (1979), "A Mathematical Introduction to Fluid Mechanics," Springer-Verlage, Berlin.

Chorin, A. J., T. J. R. Hughes, M. F. McCracken and J. E. Marsden (1978), "Product Formulas and Numerical Algorithms," Comm. on Pure and Applied Math., 31, 205-256.

Chorin, A. J. (1980), " Vortex Models and Boundary Instability," SIAM J. Scientific Stat. Comp. 1, 1-24.

Eaton, J. K. and J. P. Johnston (1980), "Turbulent Flow Reattachment: An Experimental Study of the Flow and the Structure Behind a Backward-Facing Step," Report MD-39, Stanford Univ., June 1980.

Etheridge, D. W., and P. H. Kamp (1978), "Measurement of Turbulent Flow Downstream of a Reward-Facing Step," J. Fluid Mech., 86, 545-566.

Ganji, A. R., and Sawyer, R. F. (1979), "Turbulence Combustion, Pollutant, and Stability Characterization of a Premixed Step Combustor," NASA CR-3230, 1980.

Ghoniem, A. F., A. J. Chorin, and A. K. Oppenheim (1980), "Numerical Modeling of Turbulent Flow in a Combustion Tunnel," Lawrence Berkeley Laboratory, LBL-11520.

Hald, O. H. (1979), "Convergence of Vortex Methods for Eular's Equations II. SIAM J. Numer. Anal., 16, 5, 726-755.

Hinze, J. (1975), "Turbulence."

Hsu, H. C. (1950), "Characteristics of Mean Flow and Turbulence at an Abrupt Two-Dimensional Expansion," Ph.D. Diss., Dept. of Mechanics and Hydraulics, State Univ. of Iowa.

Kim, J., S. J. Kline, and J. P. Johnston (1978), "Investigation of Separation and Reattachment of a Turbulent Shear Layer: Flow Over a Backward-Facing Step," Report MD-37, Mec. Engr., Stanford Univ.

Laufer, J. (1975), "New Trends in Experimental Turbulent Research," Annual Review of Fluid Mechanics, 7, 307-326.

Leonard, A. (1980), "Vortex Method for Flow Simulation," J. of Computational Physics, 37, 3, 1980.

McDonald, H. (1979), "Combustion Modeling in Two and Three Dimensions -- Some Numerical Considerations," Prog. Energe Combust. Sci. 5, 97-122.

Mellor, A. M. (1979), "Turbulent - Combustion Interaction Model for Practical High Intensity Combustors," 17th Symposium (international) on Combustion, the Combustion Institute, Pittsburgh, PA, 377-387.

Milne - Thomson (1976), "Theoretical Hydrodynamics."

Roshko, A. (1976). "Sturcture of Turbulent Shear Flows, A New Look," AIAA J. 14, 10, 1349-1357.

Sherman, F. S. (1976), "The Dynamics of Unstable Free Shear Layers - Effects of Buoyancy and Non-Linear Interactions," Fluid Dynamics Trans., 8, 141-193.

Sod, G. A. (1980), "Computational Fluid Dynamics With Stochastic Techniques," MAE Report No. 1479, Princeton Univ.

Taylor, C., C. E. Thomas and K. Morgan (1981), "Modeling Flow Over a Backward-Facing Step Using the F.E.M. and the Two-Equation model of Turbulence," International Journal for Numerical Method in Fluids, 1, 295-304, 1981.

Williams, F. A. and P. A. Libby (1980), "Some Implications of Recent Theoretical Studies in Turbulent Combustion," Springer Verlag, Berlin.

TABLE 3.1. - MEAN VELOCITY DISTRIBUTION ALONG BOTTOM WALL FOR HT = 1/3

[Calculated reattachment length: $X_r(Re = 10^5) = 1.93$; $X_r(Re = 10^4) = 2.22$.]

Horizontal distance, X	Velocity on edge of sheet layer, $U(\delta)$	
	$Re = 10^5$	$Re = 10^4$
0.1	-0.143	-0.076
.3	- .701	- .061
.5	-1.154	- .286
.7	-1.209	- .354
.9	-1.193	- .352
1.1	-1.019	- .323
1.3	- .759	- .282
1.5	- .304	- .391
1.7	- .134	- .279
1.9	- .033	- .262
2.1	.174	- .021
2.3	.152	.015
2.5	.148	.026
2.7	.314	.081

TABLE 3.2. - COMPARISON OF VORTEX NUMBER WITH DIFFERENT INLET LENGTH FOR HT = 1/3

Time step	No. of vortex blobs in channel, NV	No. of vortex sheet on horizontal top wall, NSA	No. of vortex sheet on horizontal bottom inlet wall, NSB	No. of vortex sheet on vertical wall, NSC	No. of vortex sheet on horizontal bottom wall in channel, NSD
		Inlet length of channel, X(in), 1.0			
10	43	135	28	1	104
20	102	182	36	3	155
30	192	243	45	3	208
40	301	311	37	4	240
50	437	388	33	5	295
60	554	431	46	6	328
70	647	497	29	4	367
80	757	612	38	10	432
90	920	635	33	7	468
100	1013	708	33	6	510
		Inlet length of channel, X(in), 3.0			
10	55	174	77	5	83
20	165	276	116	9	125
30	272	367	140	9	183
40	431	449	172	1	224
50	620	526	204	3	276
60	867	667	232	8	290
70	1117	743	266	6	343
80	1351	896	262	7	387
90	1533	954	267	4	471
100	1677	1054	273	5	507

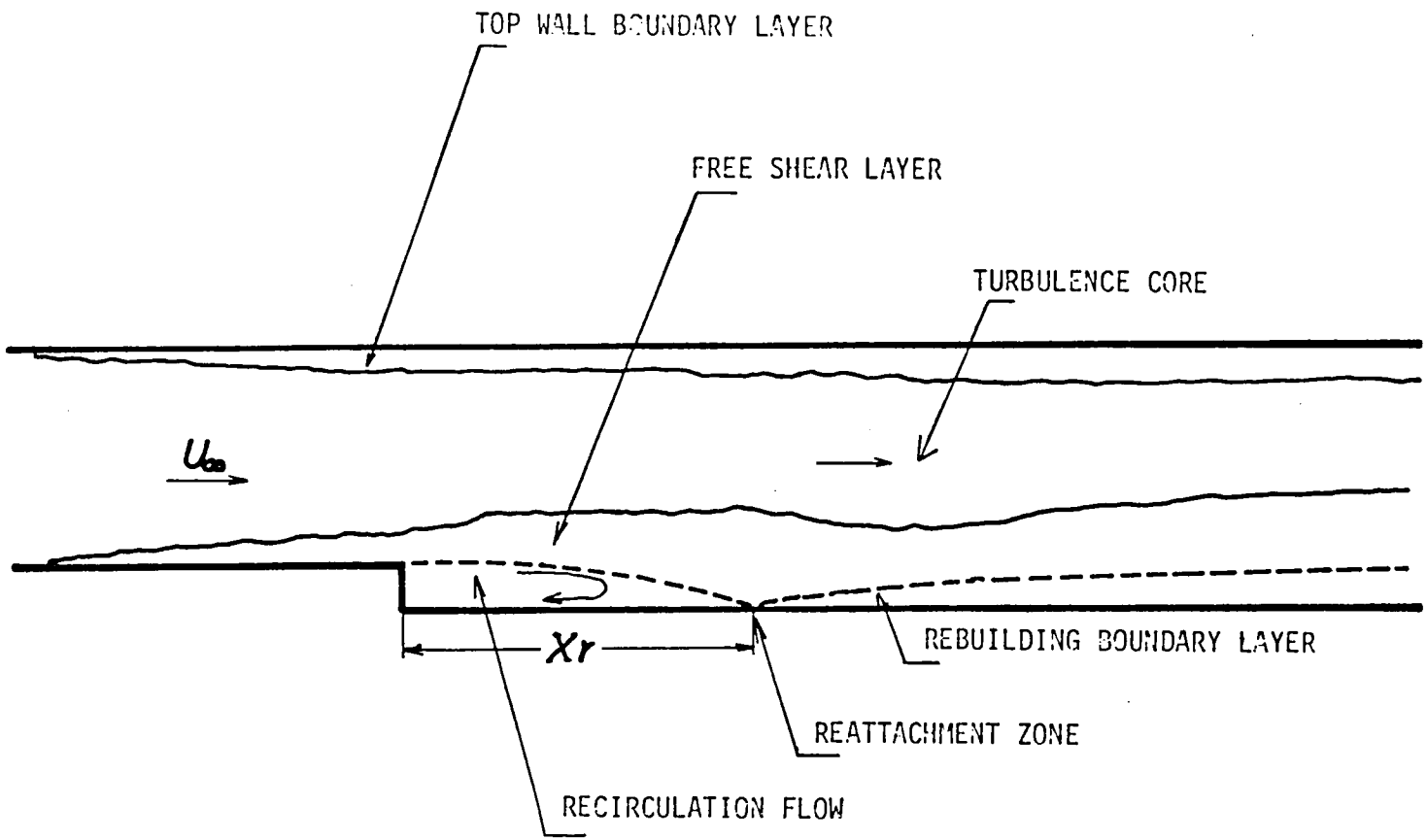

Figure 1. - Illustration of backward-facing step flow field.

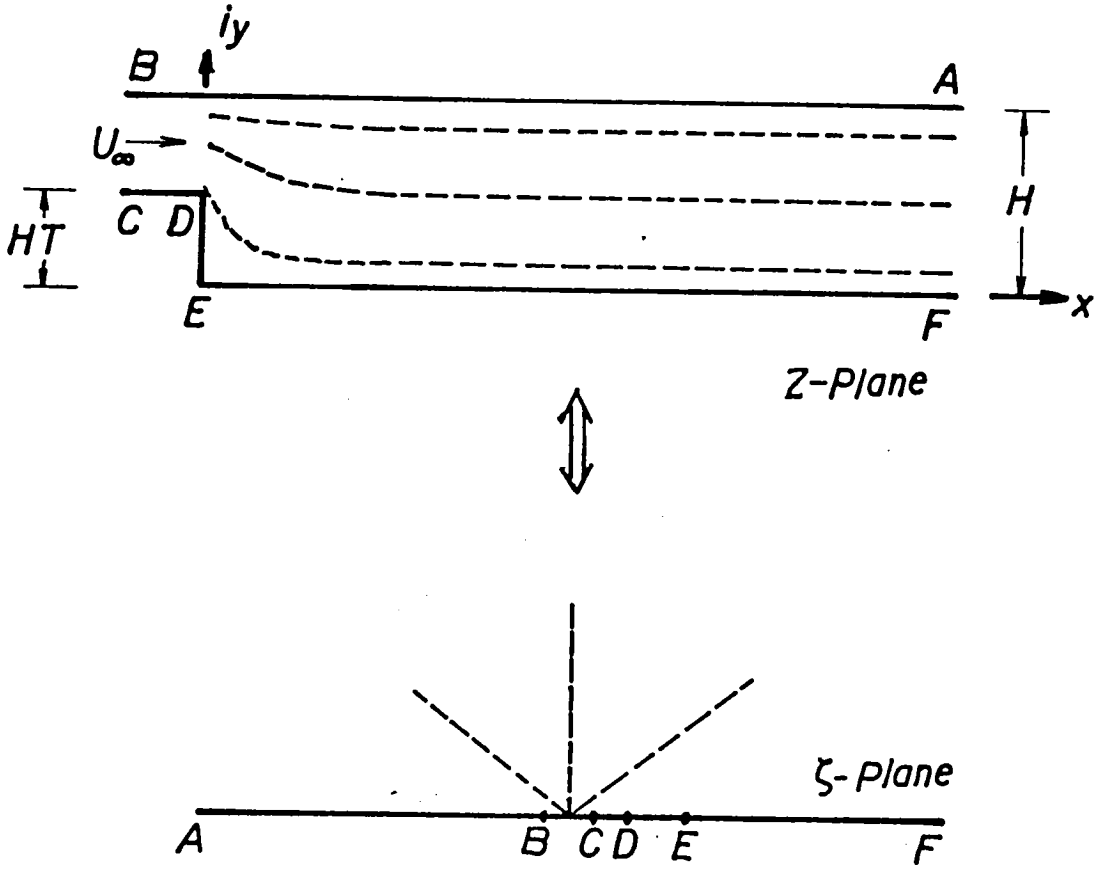

Figure 2.1. - Illustration of conformal mapping.

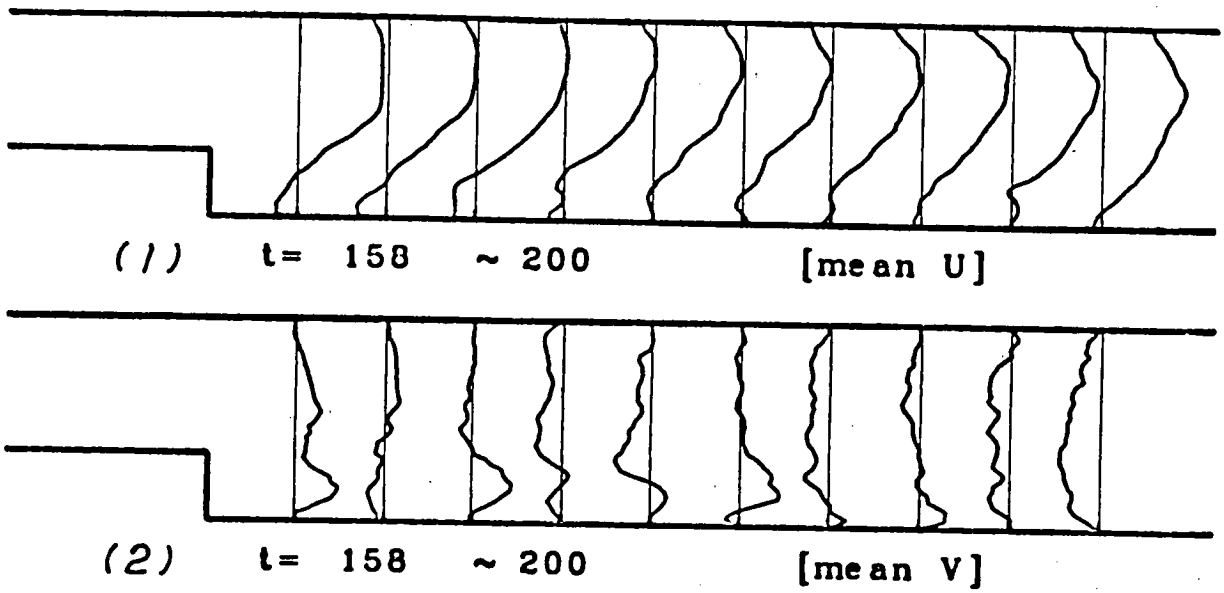

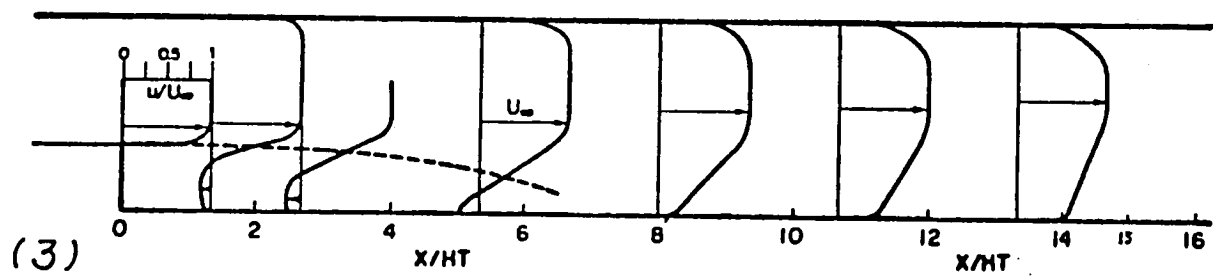

Figure 3.1(a). - Mean velocity profile along channel with HT = 1/3.
(1)-(2) Numerical data of time steps 158 to 200 at Re = 10^4.
(3) Experimental data from J. Kim.

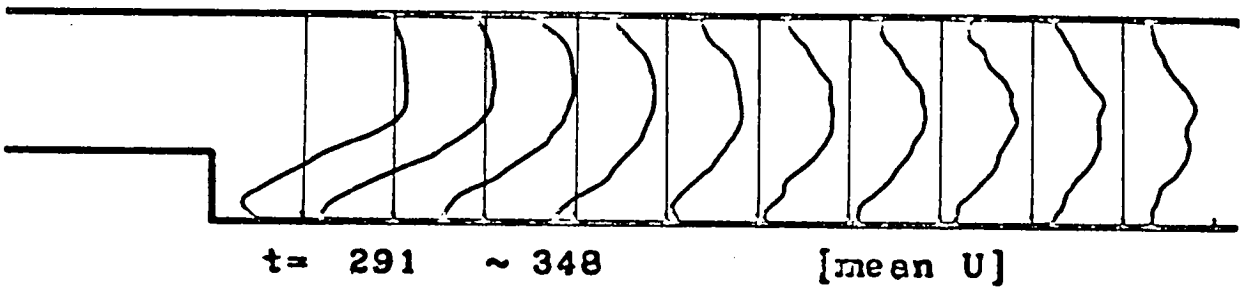

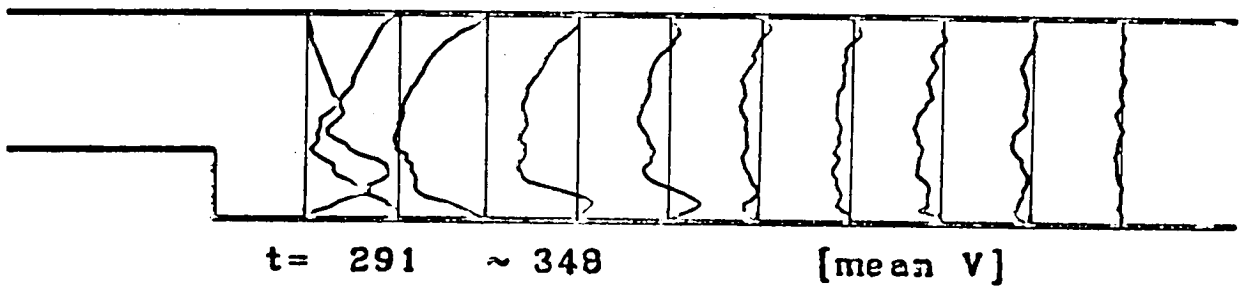

Figure 3.1(b). - Mean velocity profile along channel with HT + 1/3 between time steps 291 to 348 at Re = 10^4.

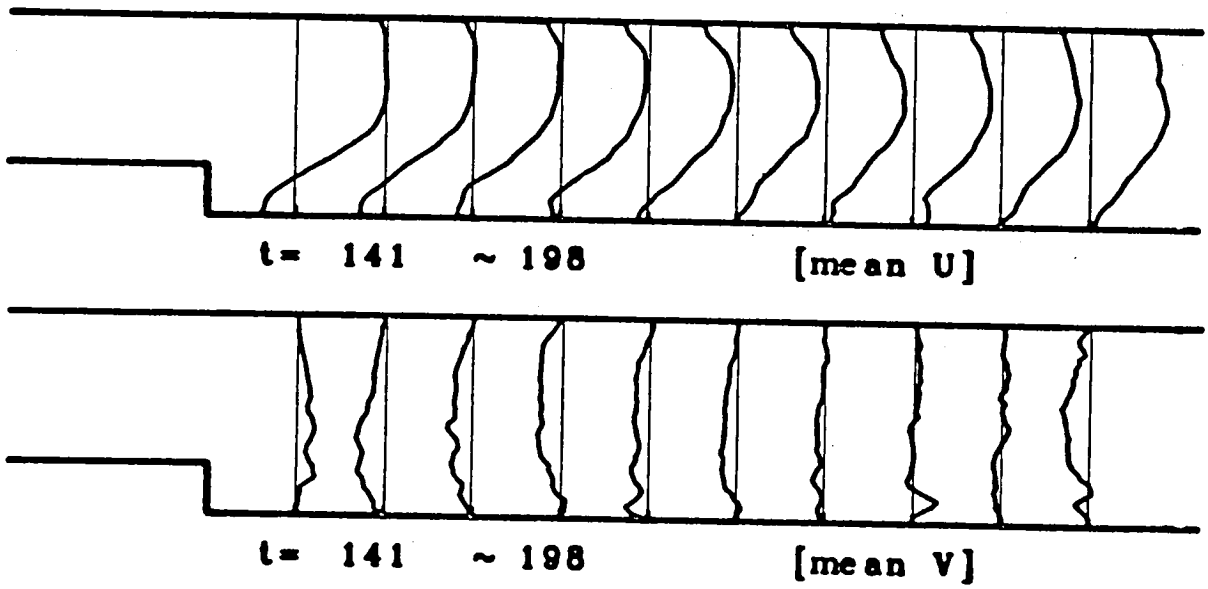

Figure 3.2. - Mean velocity along channel with HT = 1/4, Re = 10^4, and time steps 141 to 198.

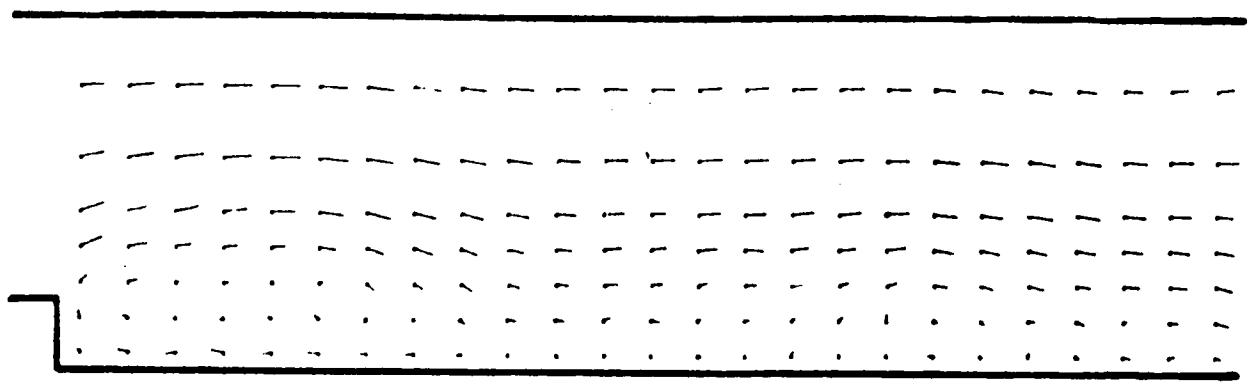

Figure 3.3. - Mean velocity profile along channel with HT = 1/5, Re = 10^4, and time steps 140 to 172.

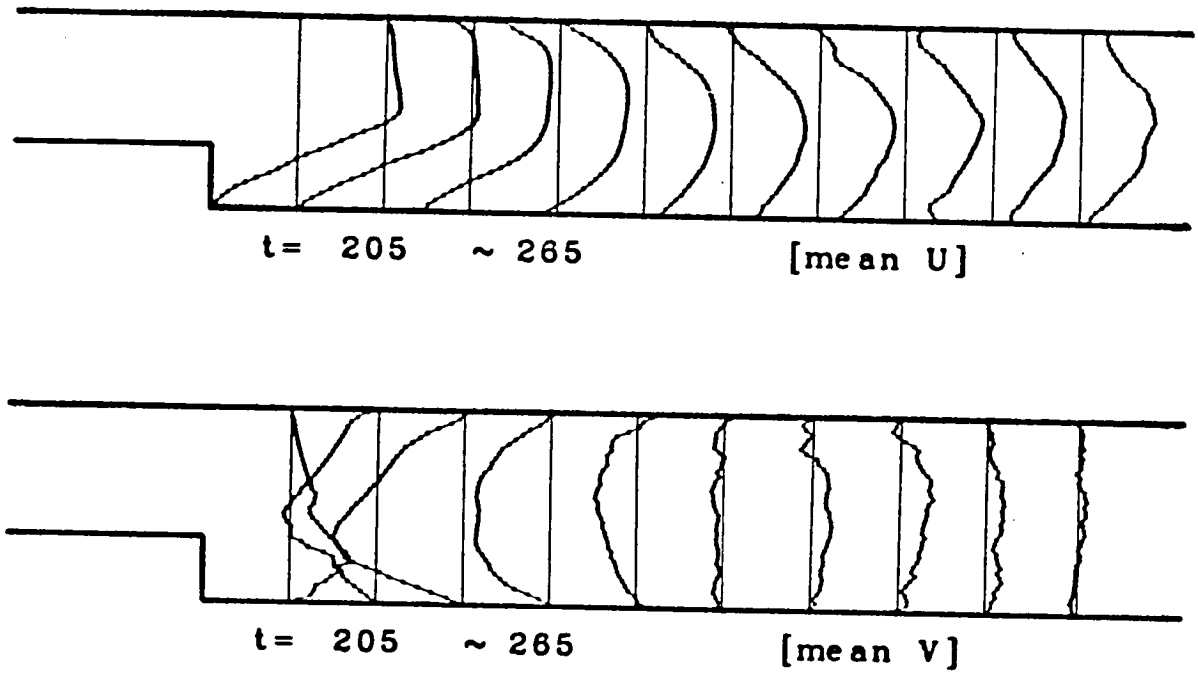

Figure 3.4. – Mean velocity profile along channel with HT = 1/3, Re = 10^5, and time steps 205 to 265.

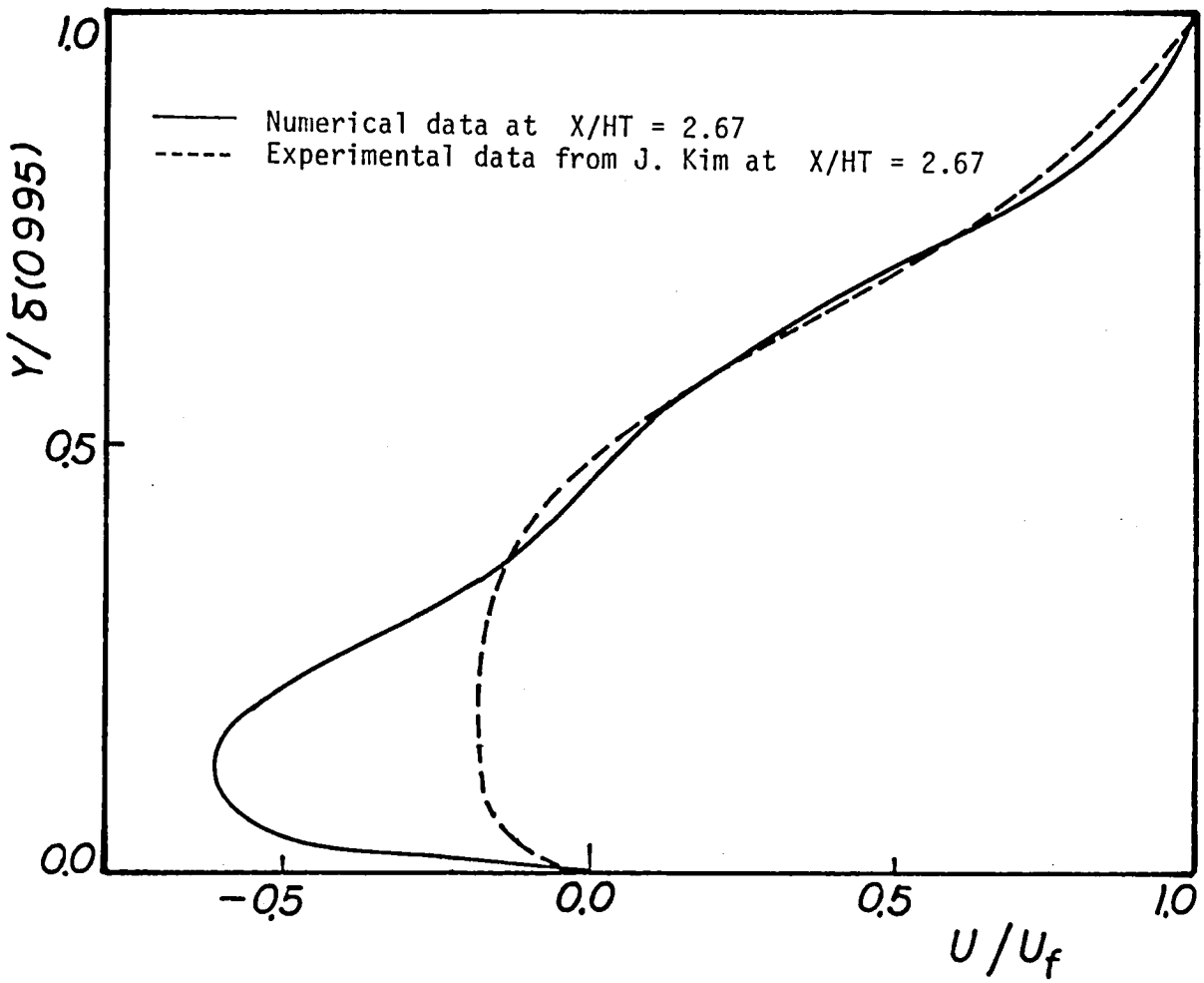

Figure 3.5. - Mean velocity profile on step side between time steps 158 to 200 with HT = 1/3 and Re = 10^4.

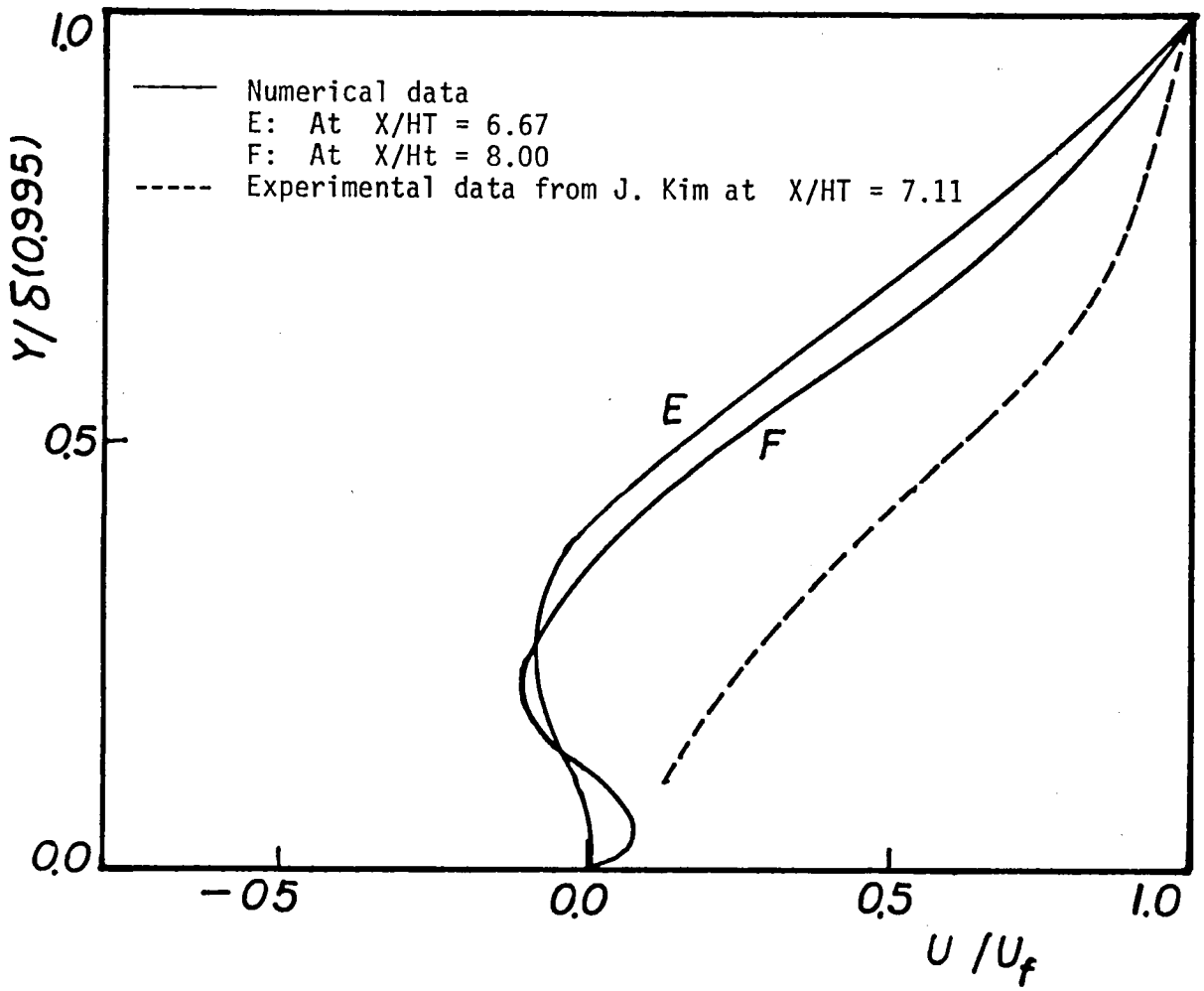

Figure 3.6. - Mean velocity profiles on step side between time steps 158 to 200 with HT = 1/3 and Re = 10^4.

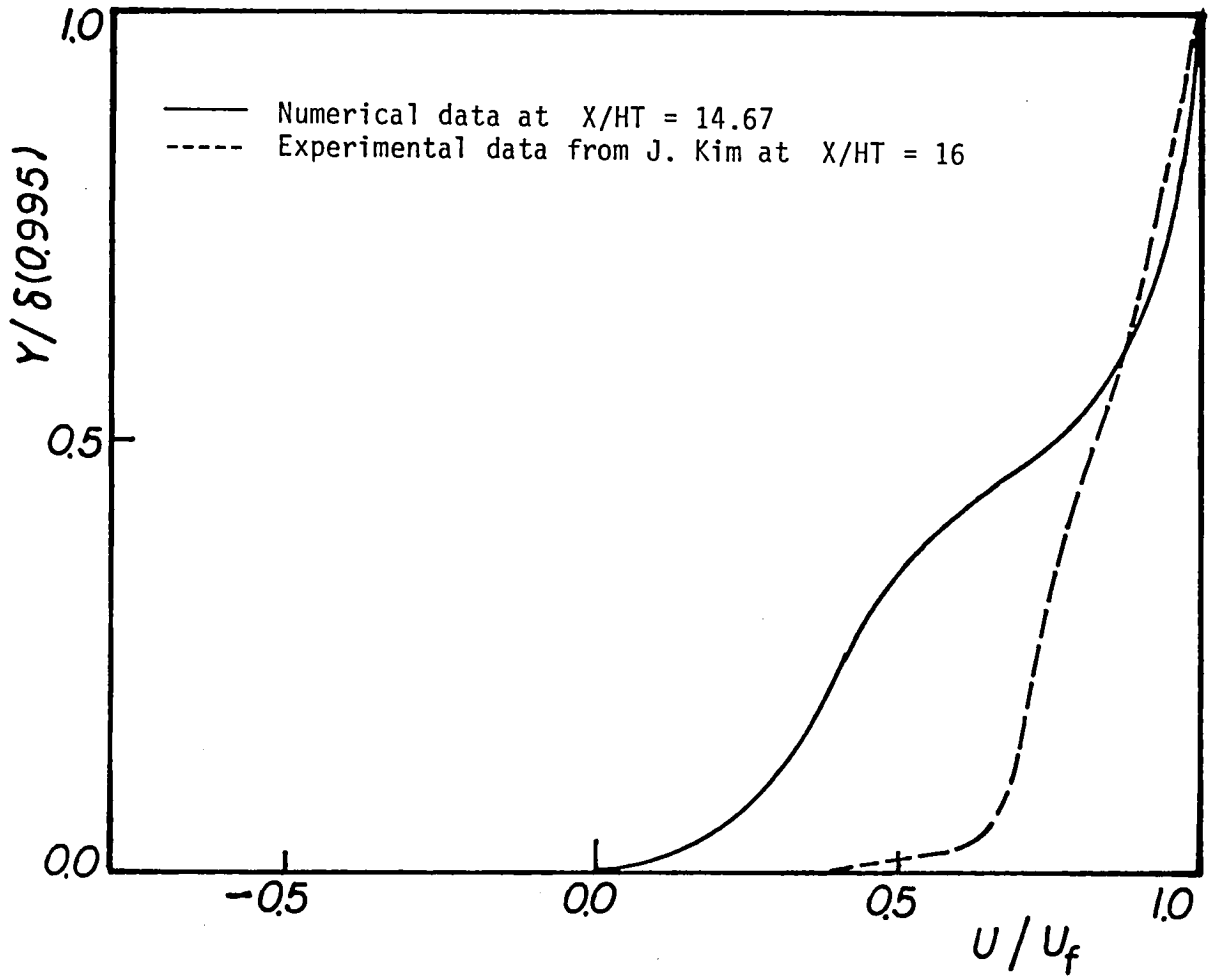

Figure 3.7. - Mean velocity profile on step side between time steps 158 to 200 with HT = 1/3 and Re = 10^4.

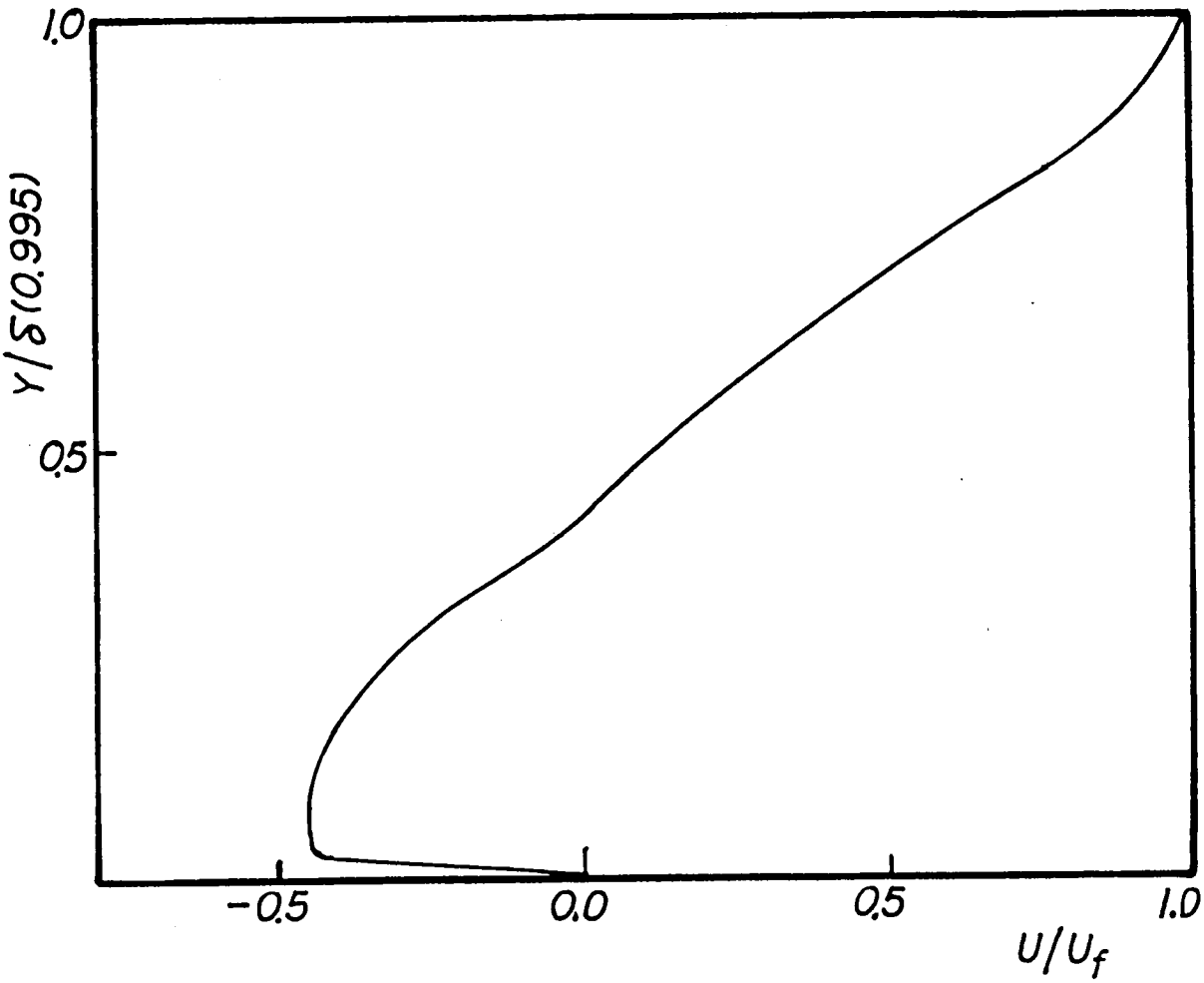

Figure 3.8. - Mean velocity profile on step side between time steps 141 to 198 with HT = 1/4, Re = 10^4, and X/HT = 3.56.

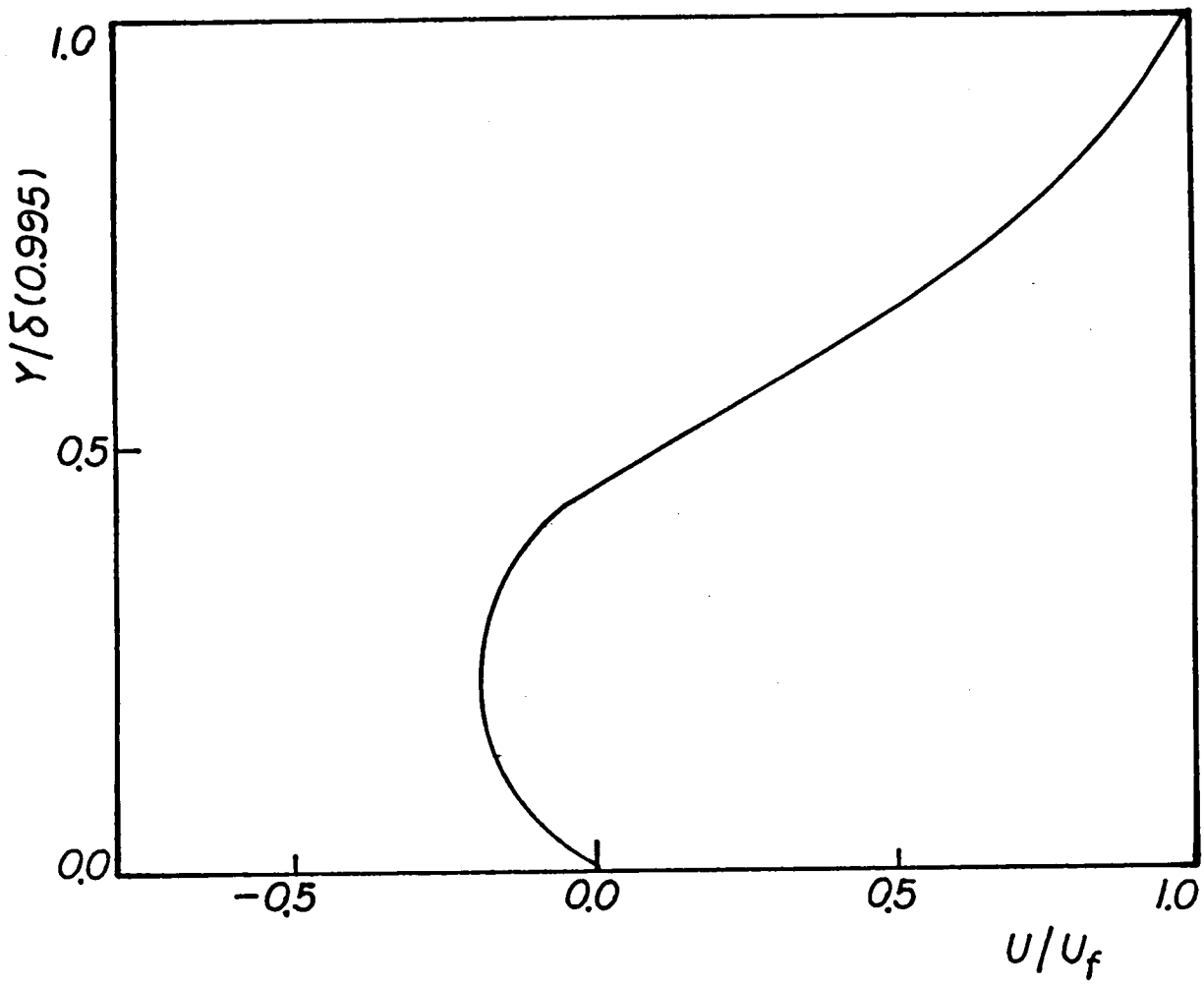

Figure 3.9. - Mean velocity profile on step side between time steps 141 to 198 with HT = 1/4, Re = 10^4, and X/HT = 7.11.

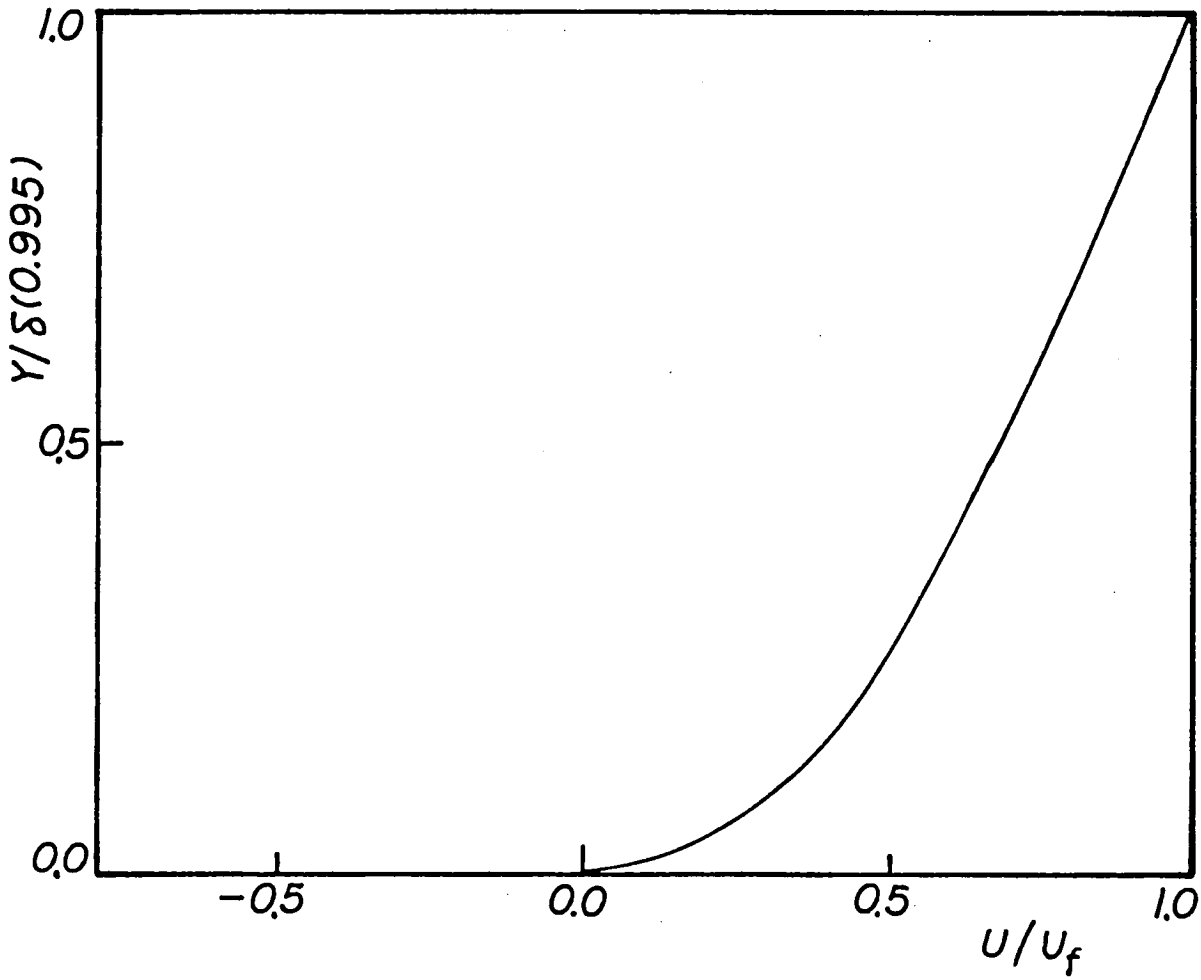

Figure 3.10. - Mean velocity profile on step side between time steps 141 to 198 with HT = 1/3, Re = 10^4, and X/HT = 19.56.

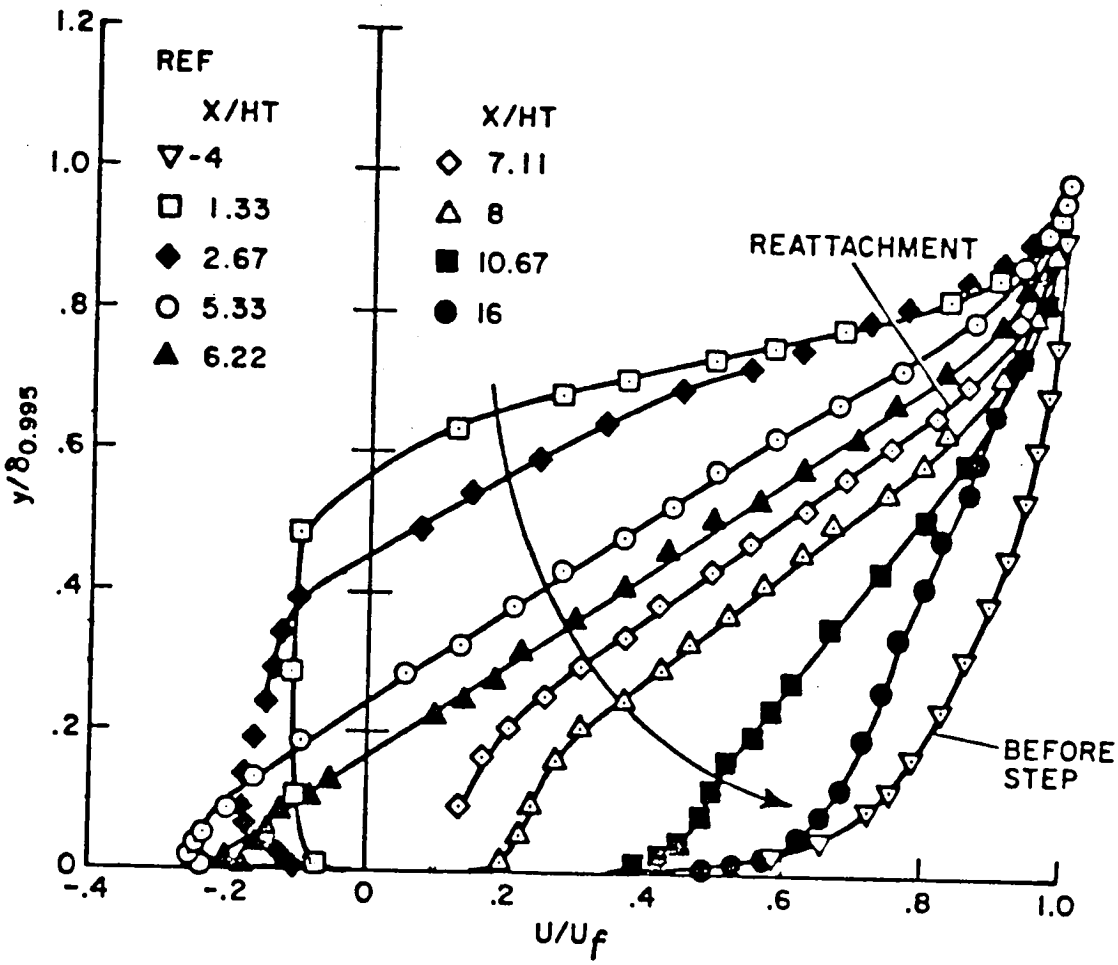

Figure 3.11. – Velocity profiles on step side with U/U_f as function of y/δ; experimental data from J. Kim.

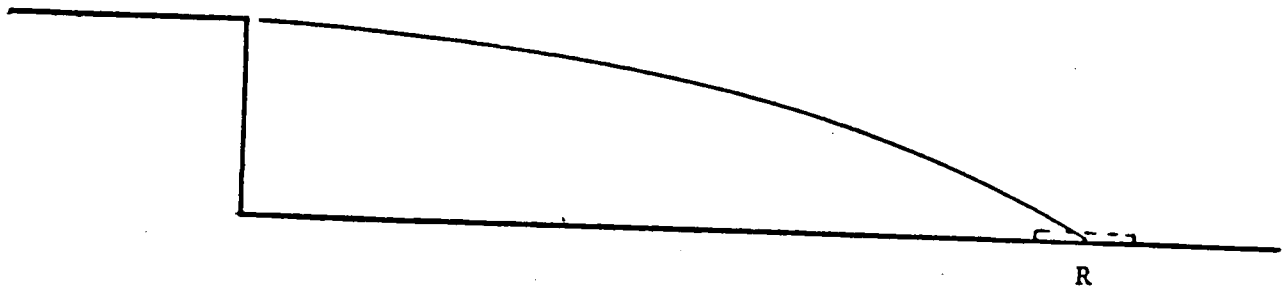

$(\partial\tau/\partial y)dxdy - (\partial p/\partial x)dxdy = 0$

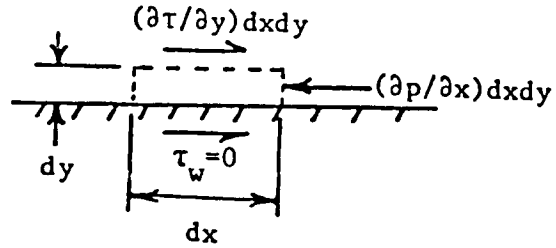

Figure 3.12. - Control volume at reattachment point.

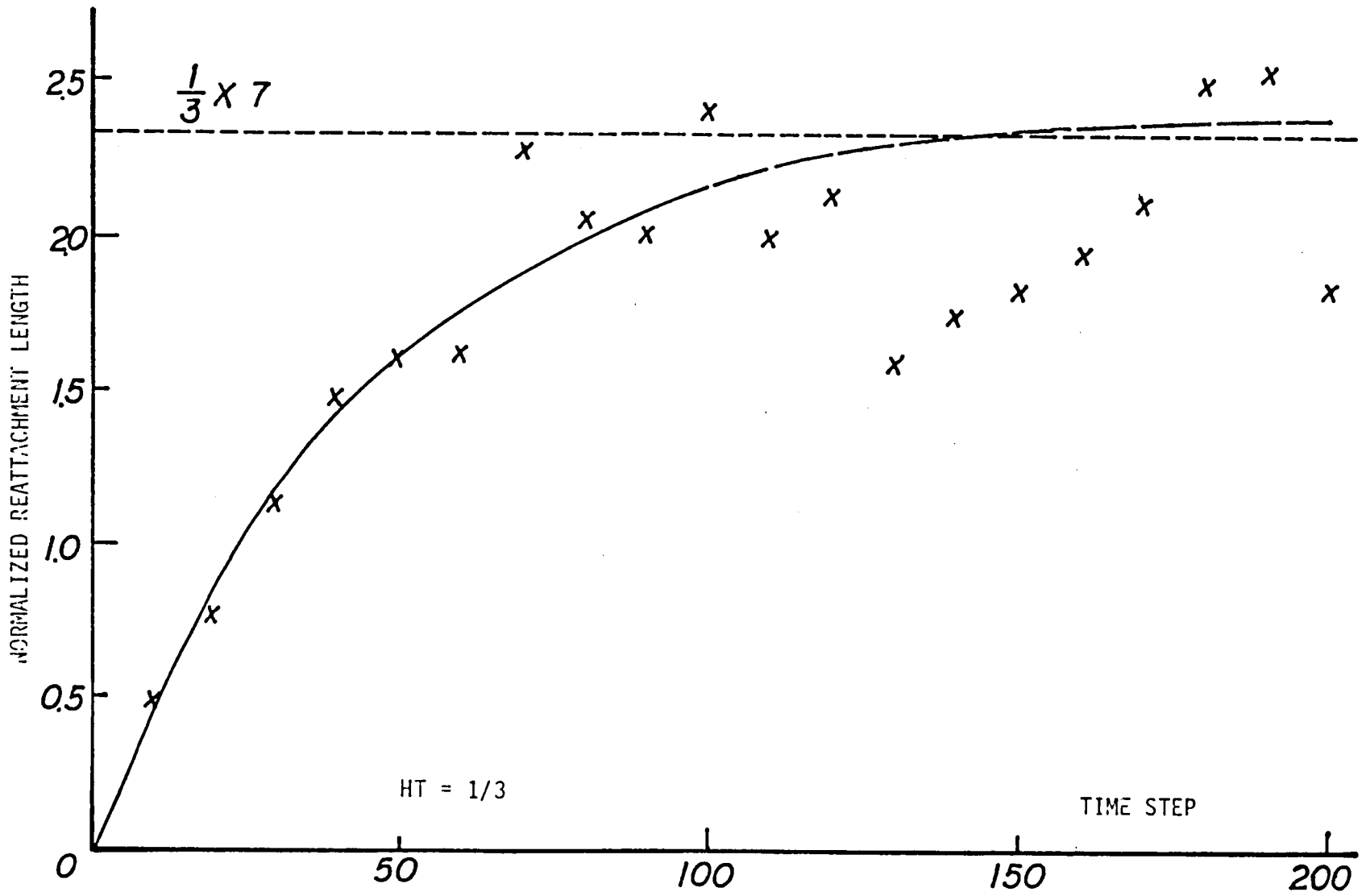

Figure 3.13. - Development of reattachment zone.

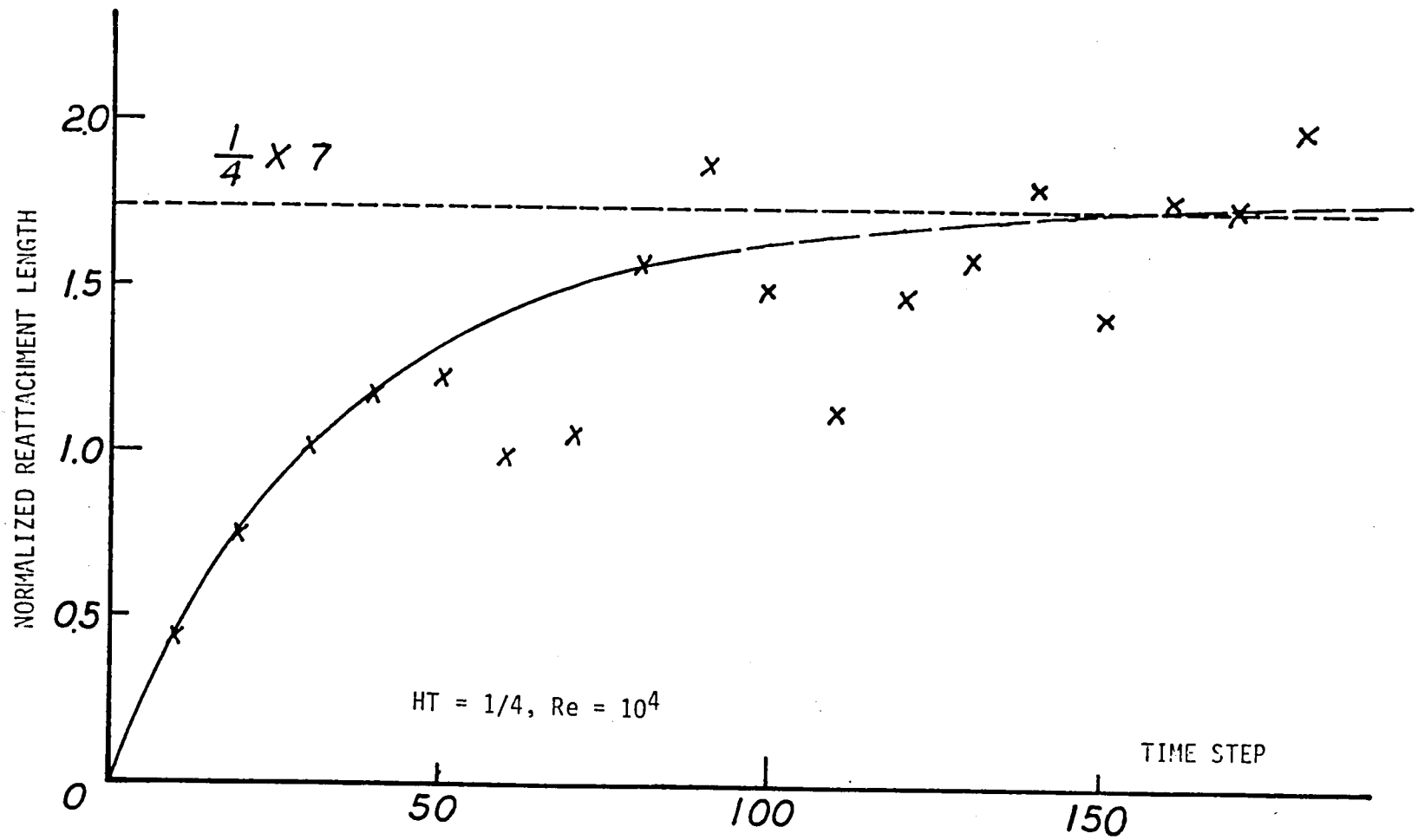

Figure 3.14. – Development of reattachment zone.

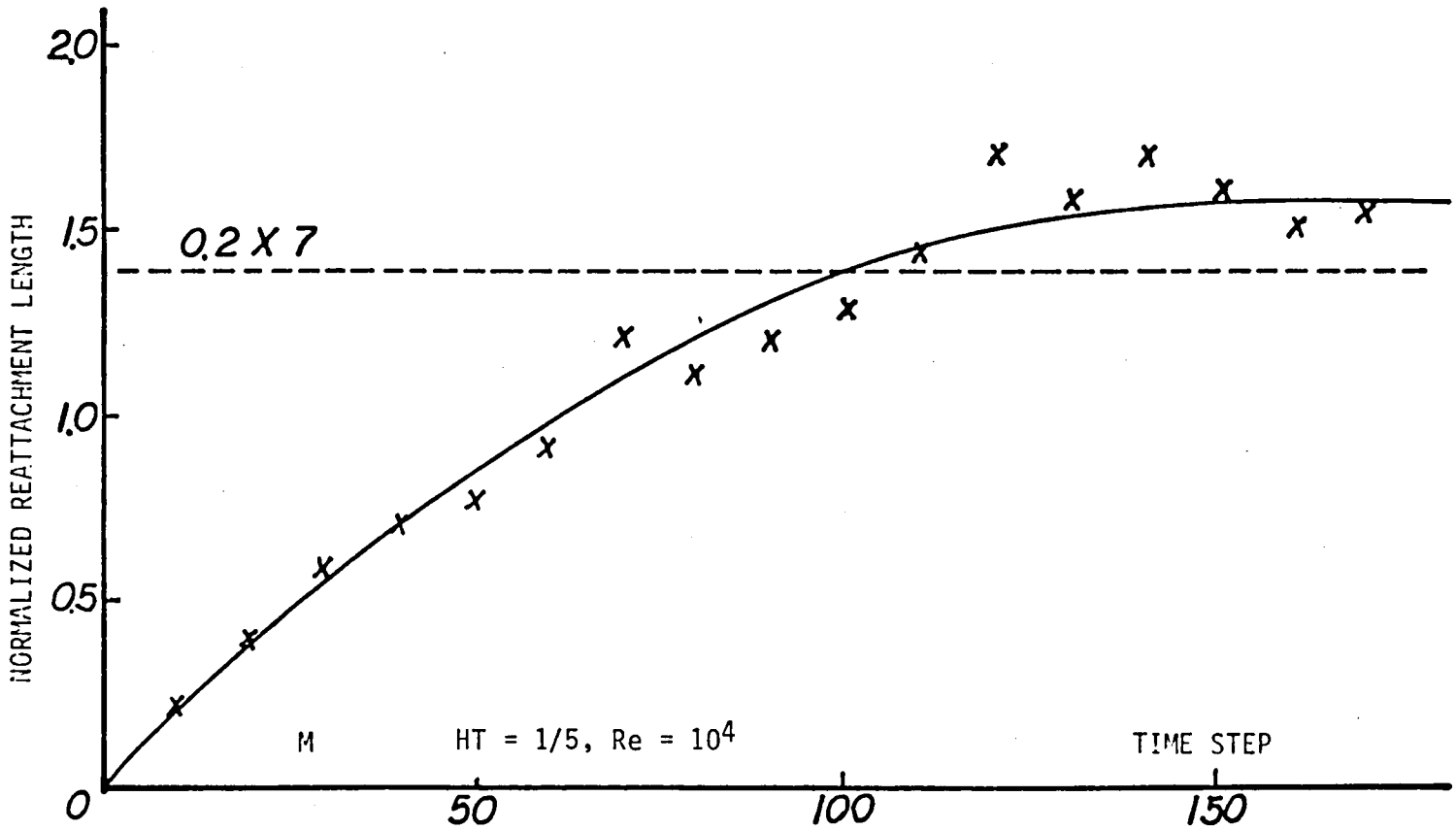

Figure 3.15. - Development of reattachment zone.

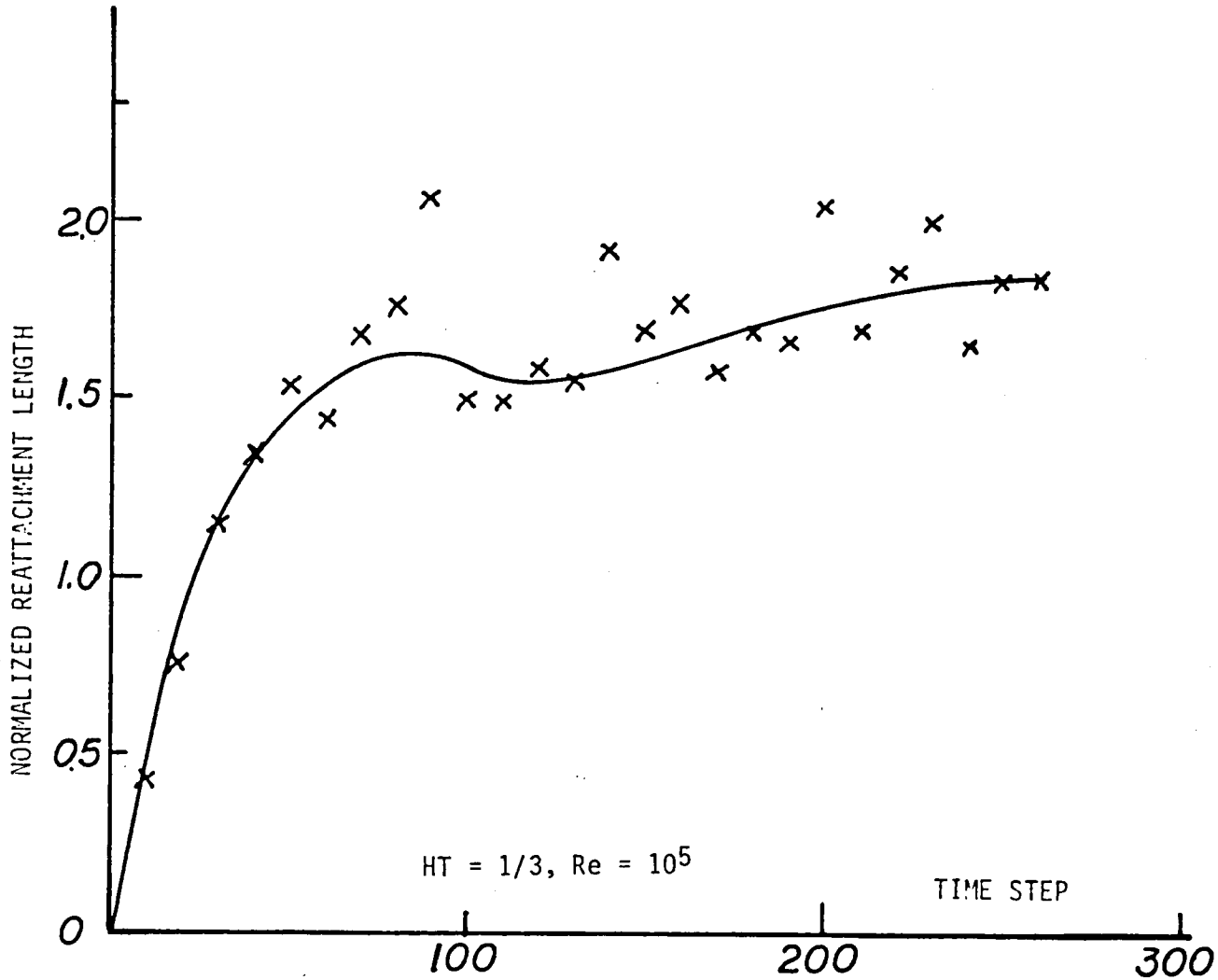

Figure 3.16. - Development of reattachment zone.

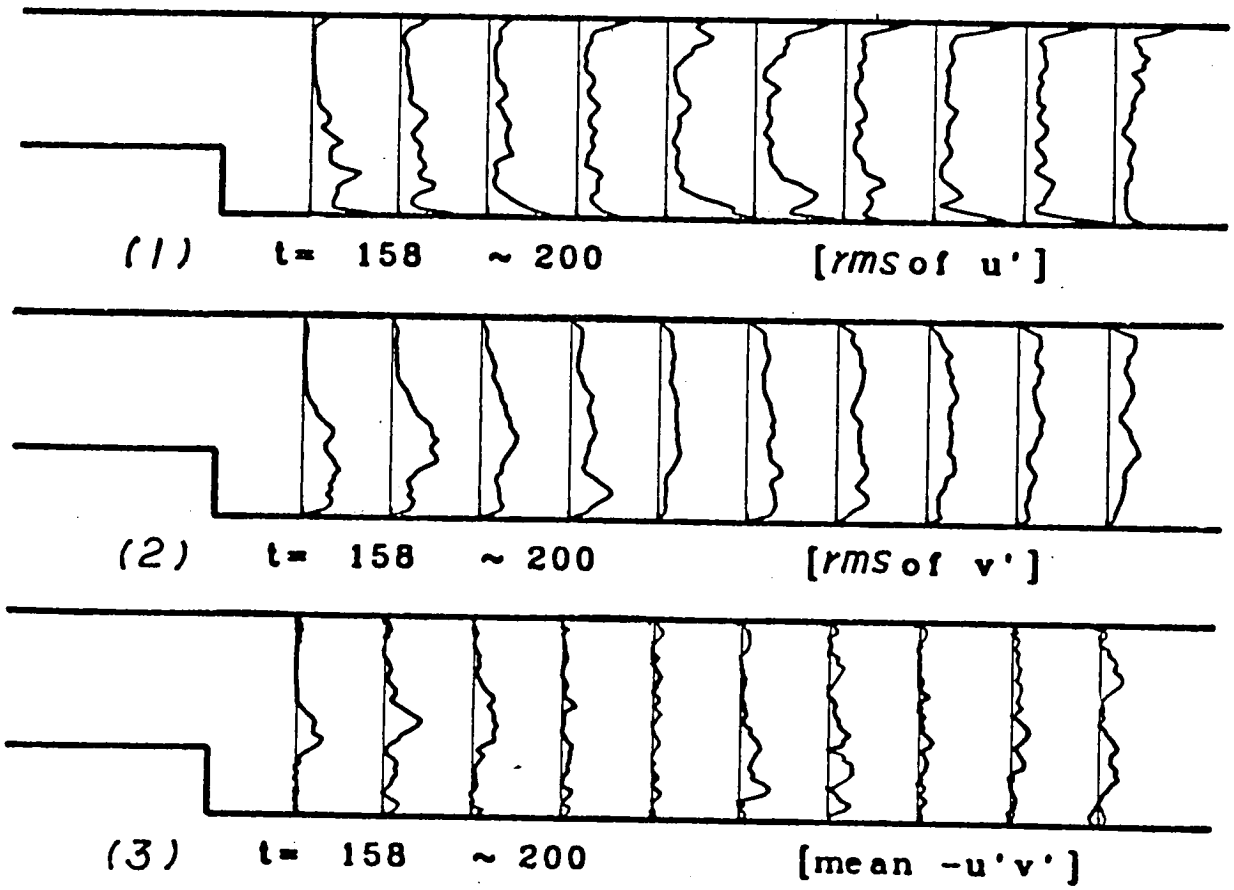

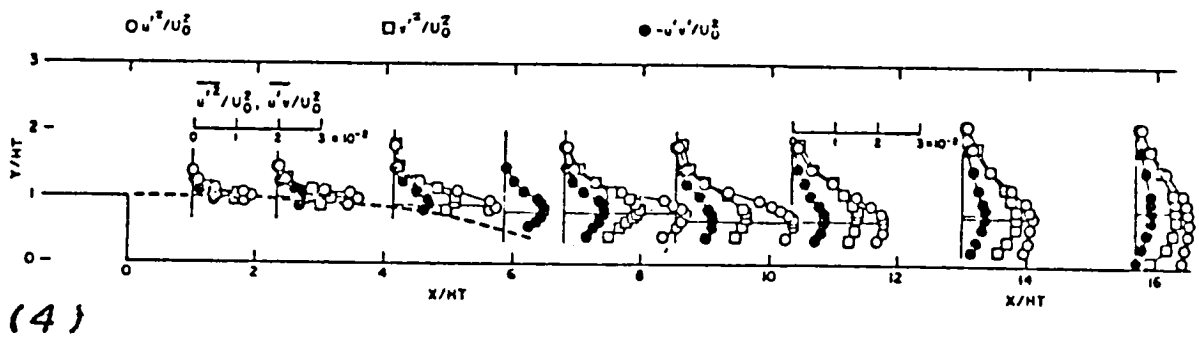

(4)

Figure 3.17(a). - Mean turbulence profile along channel with HT = 1/3.
(1)-(3) Numerical data of time steps 158 to 200 at Re = 10^4.
(4) Experimental data from J. Kim.

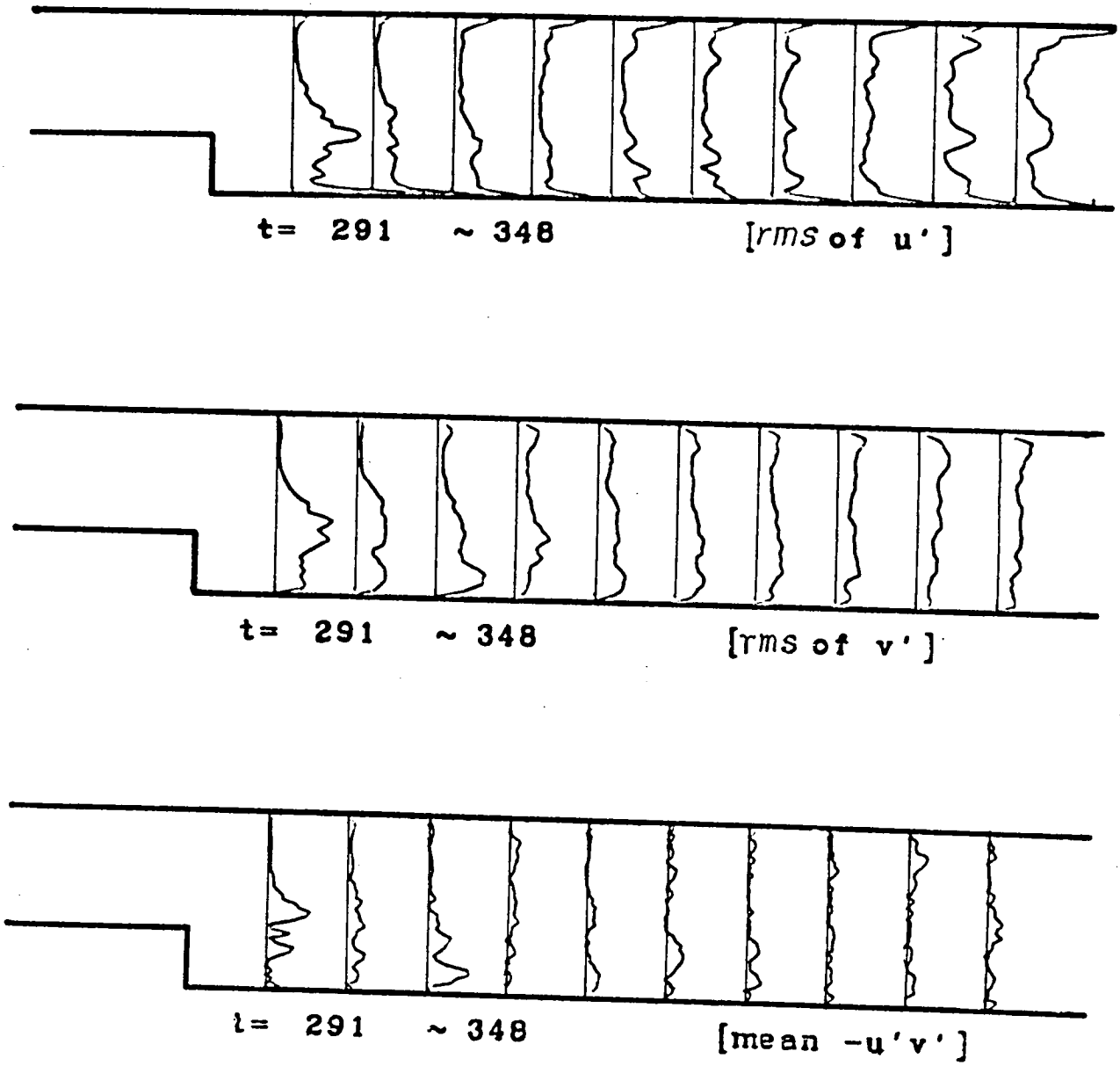

Figure 3.17(b). - Mean turbulence profile along channel with HT = 1/3 between time steps 290 to 348 at $Re = 10^4$.

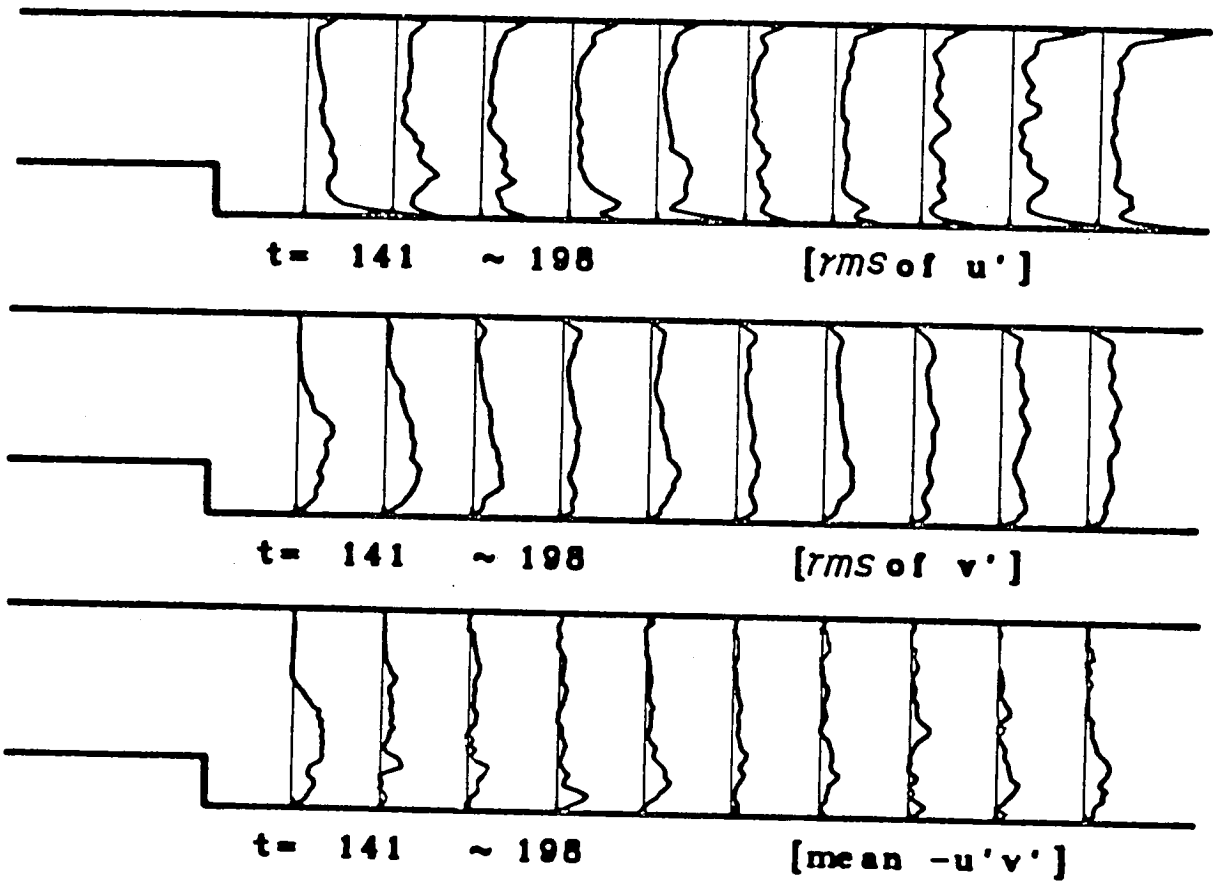

Figure 3.18. - Mean turbulence profiles in channel with HT = 1/4, Re = 10^4 between time steps 141 to 198.

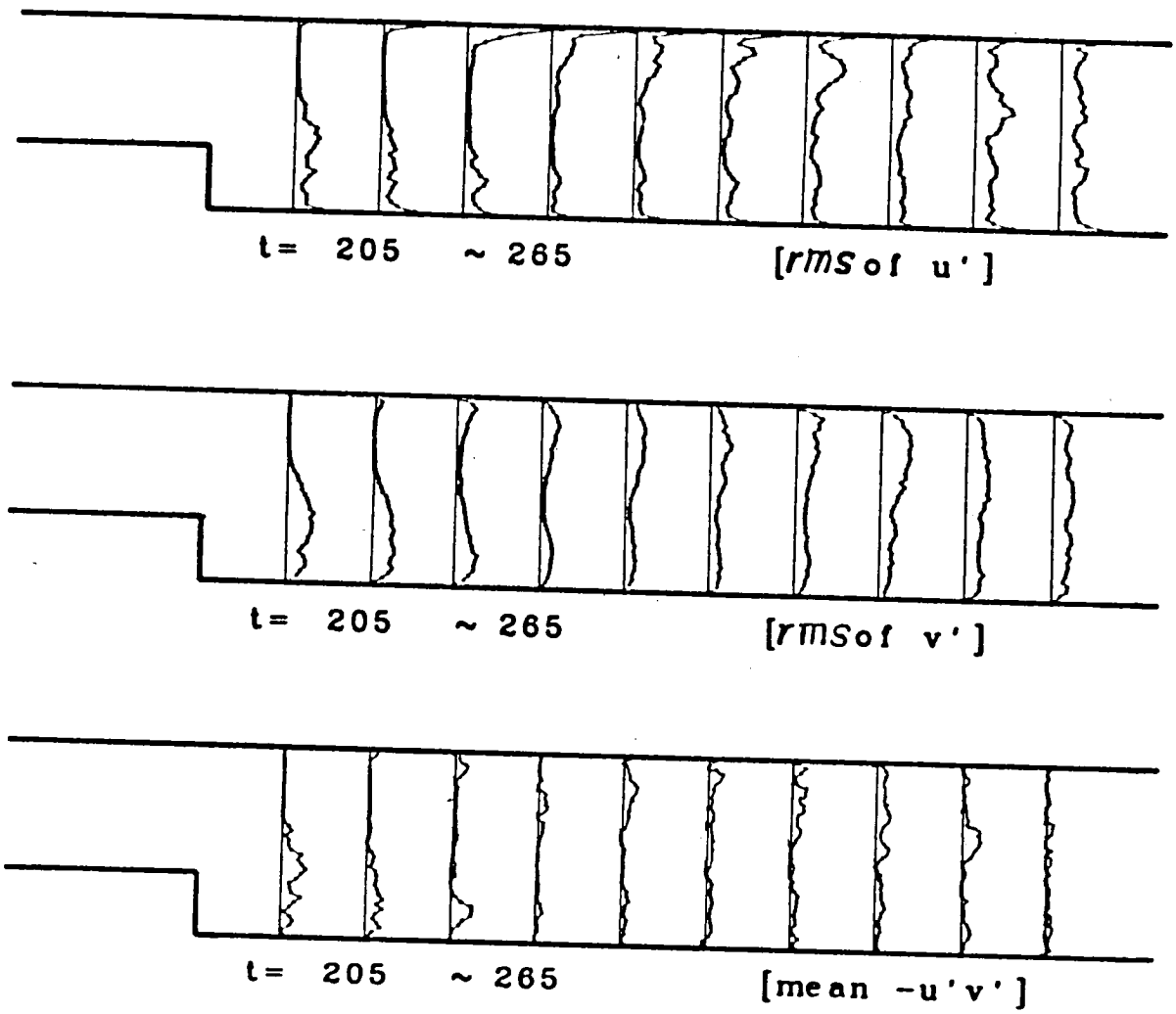

Figure 3.19. - Mean turbulence profile along channel with HT = 1/3, Re = 10^5, and time steps 205 to 265.

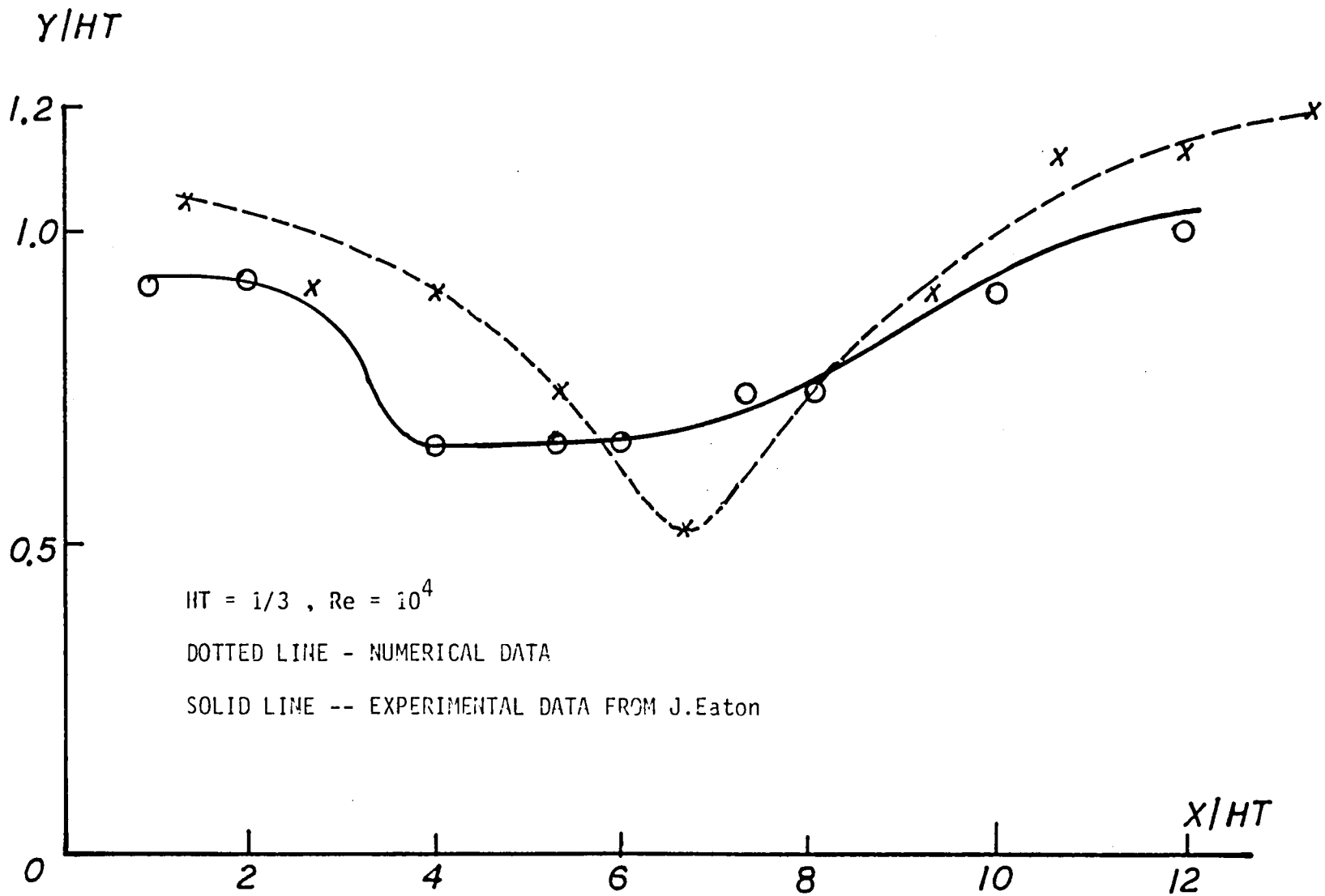

Figure 3.20. - Location of maximum turbulence intensity.

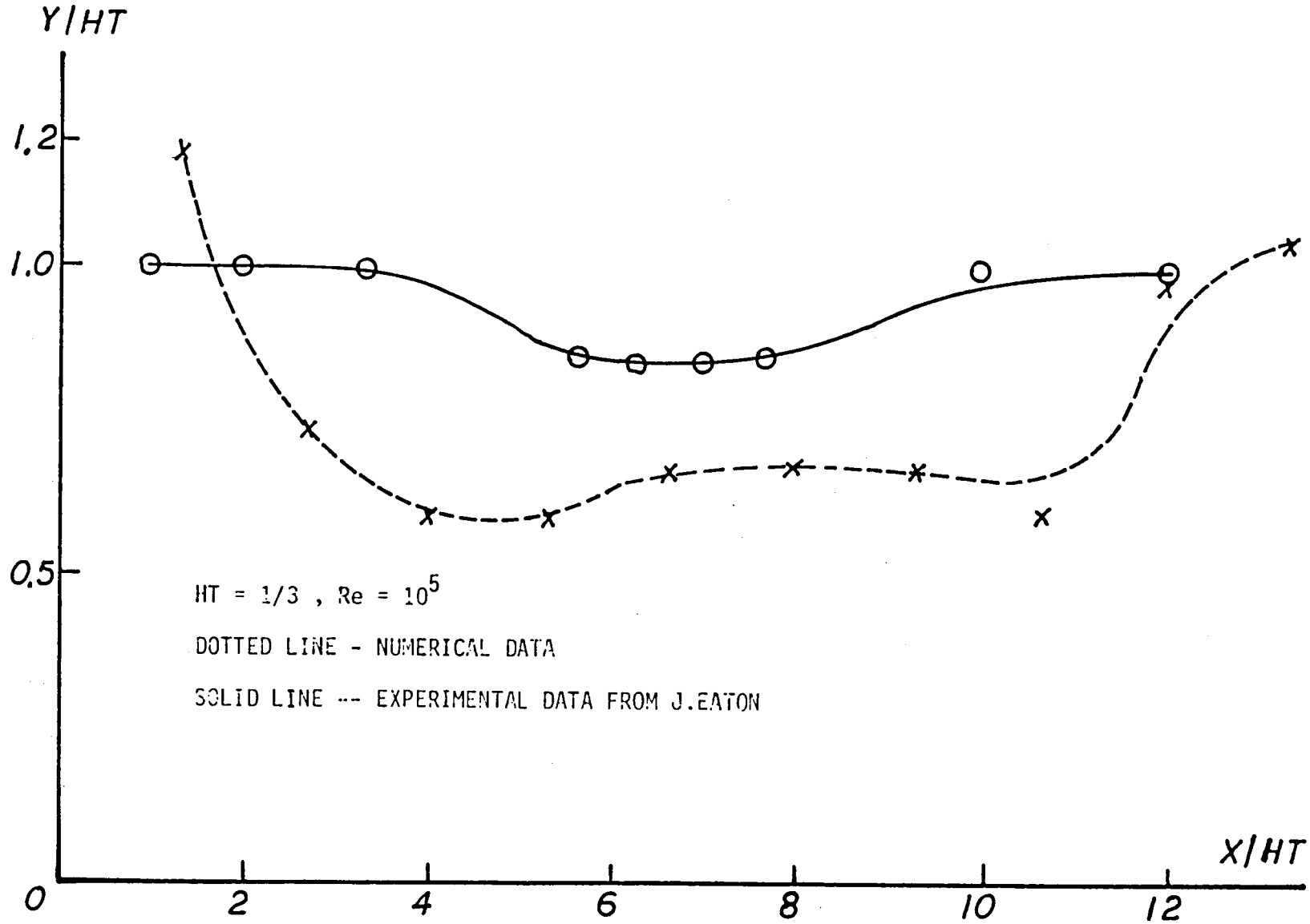

Figure 3.21. - Location of maximum turbulence intensity.

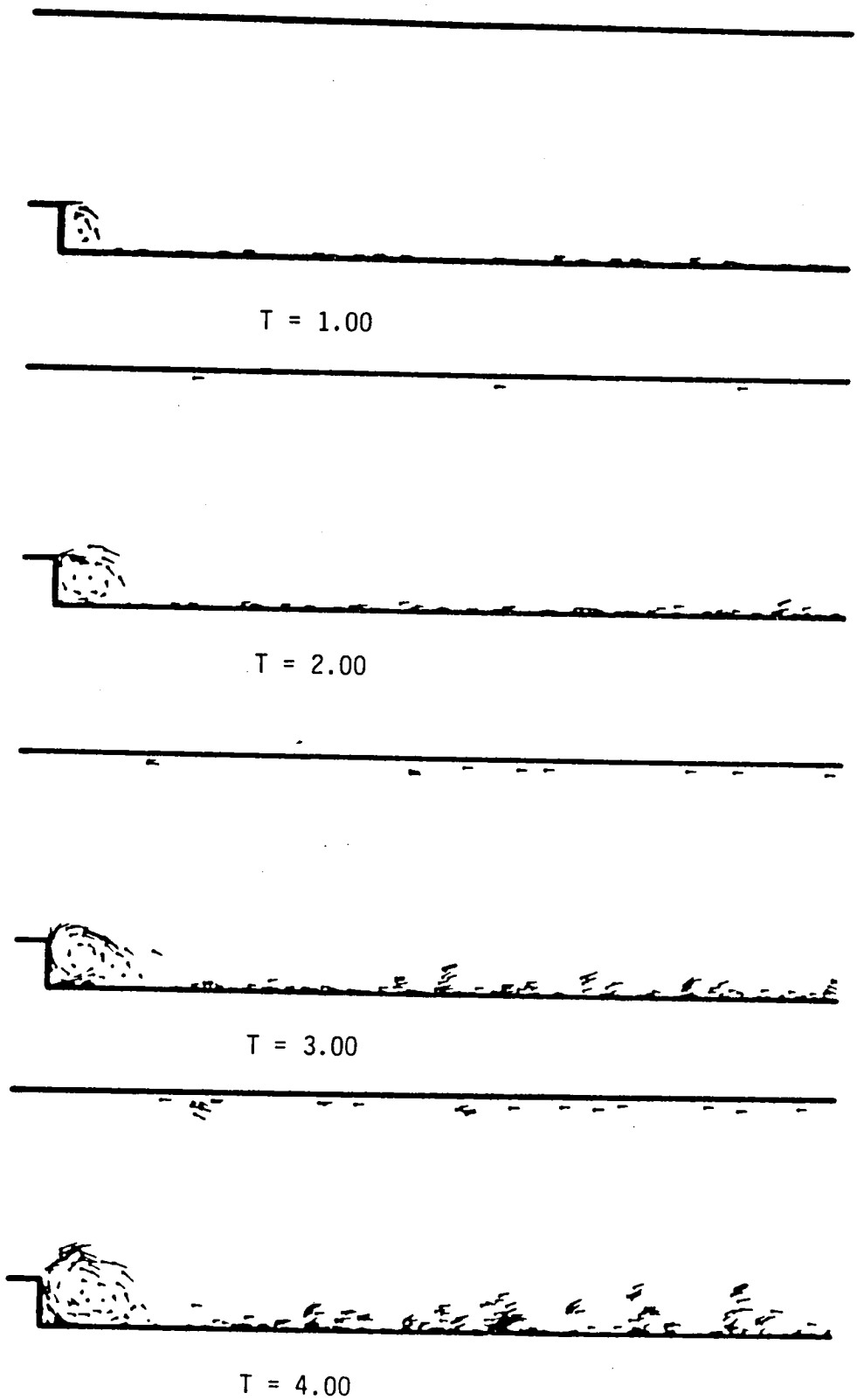

Figure 3.22. - Flow development along channel at HT = 1/5 and Re = 10^4.

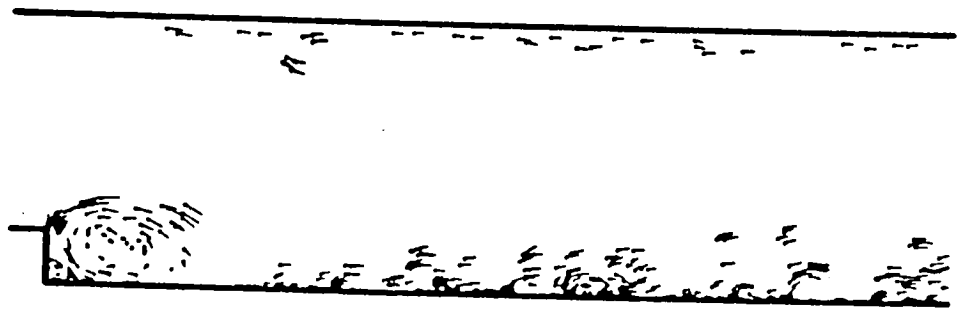

T = 5.00

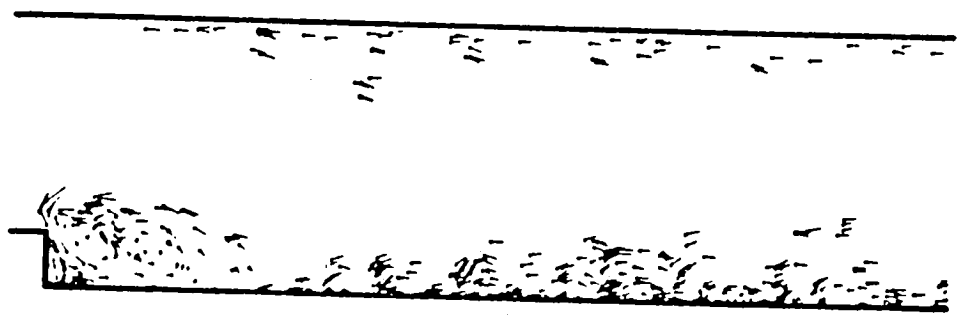

T = 6.00

T = 7.00

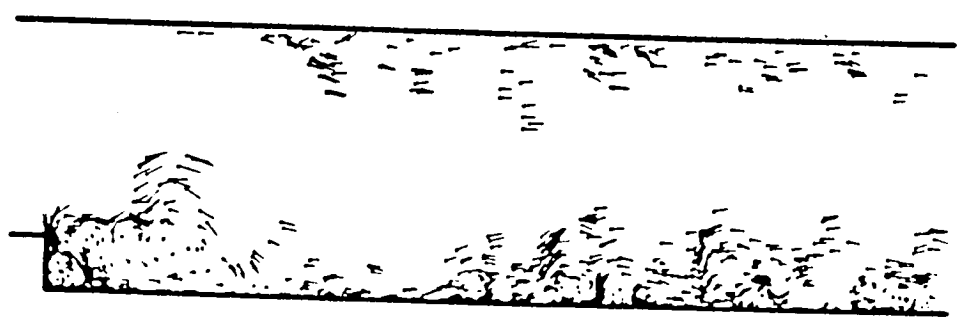

T = 8.00

Figure 3.22(b). - Continued.

T = 9.00

T = 10.00

T = 11.00

Figure 3.22(c). - Continued.

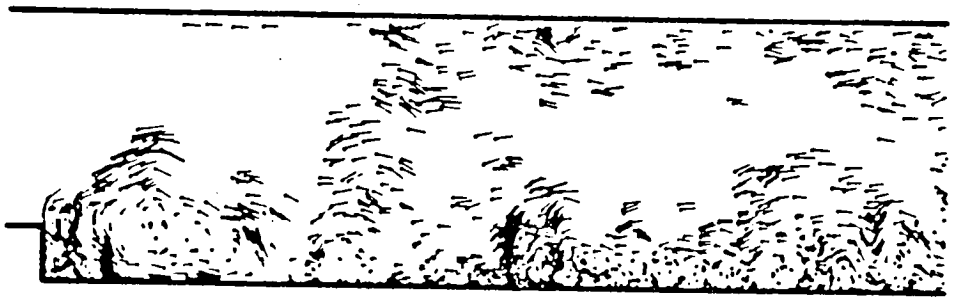

T = 12.00

T = 13.00

T = 14.00

Figure 3.22(d). - Continued.

T = 15.00

T = 16.00

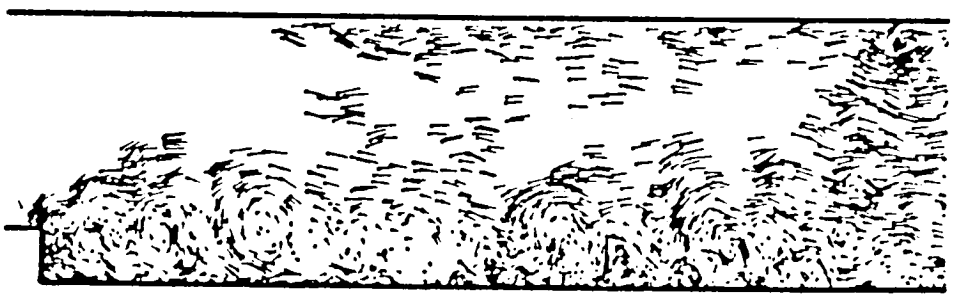

T = 17.00

Figure 3.22(e). - Concluded.

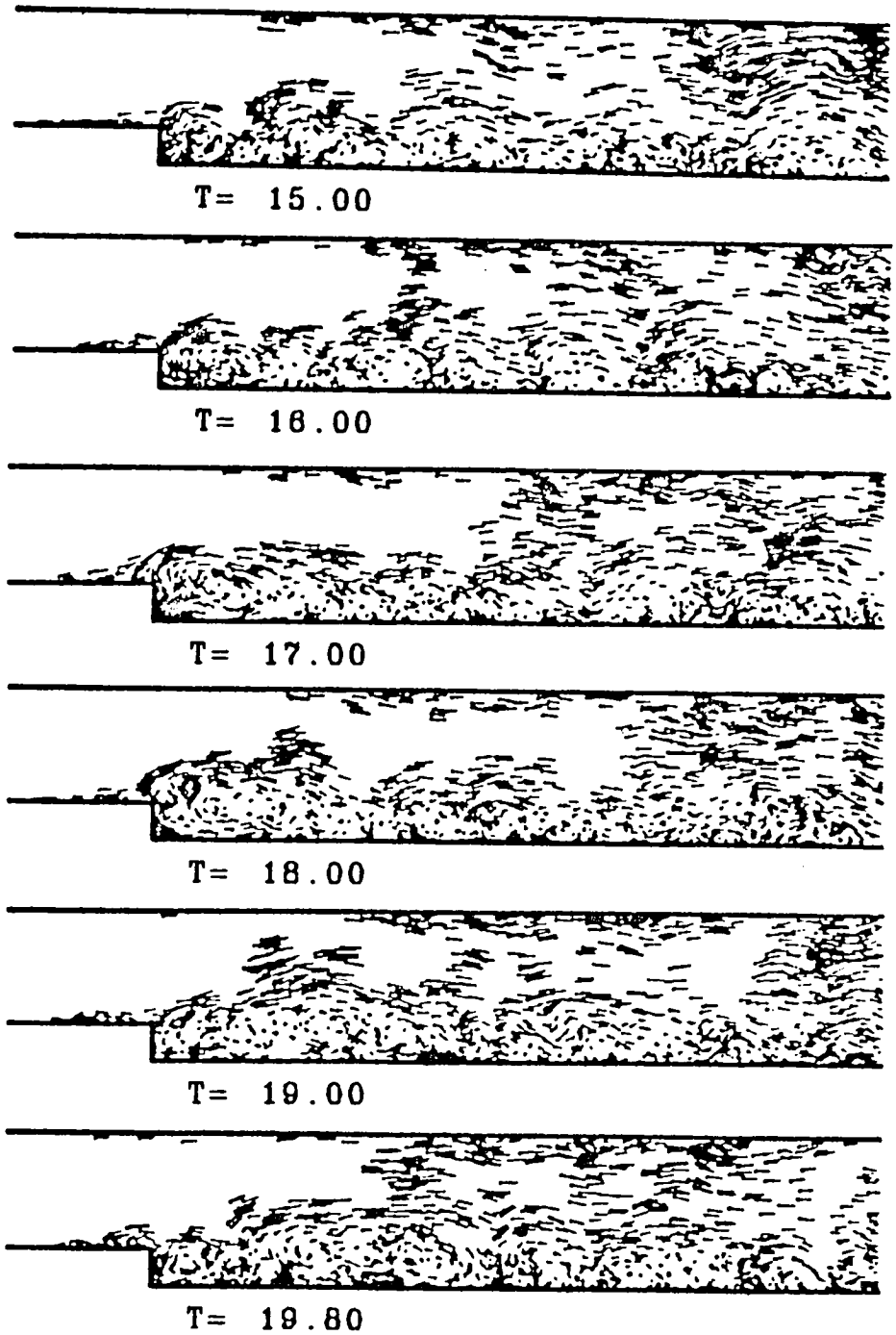

Figure 3.23. - Flow development along channel at HT = 1/4 and Re = 10^4.

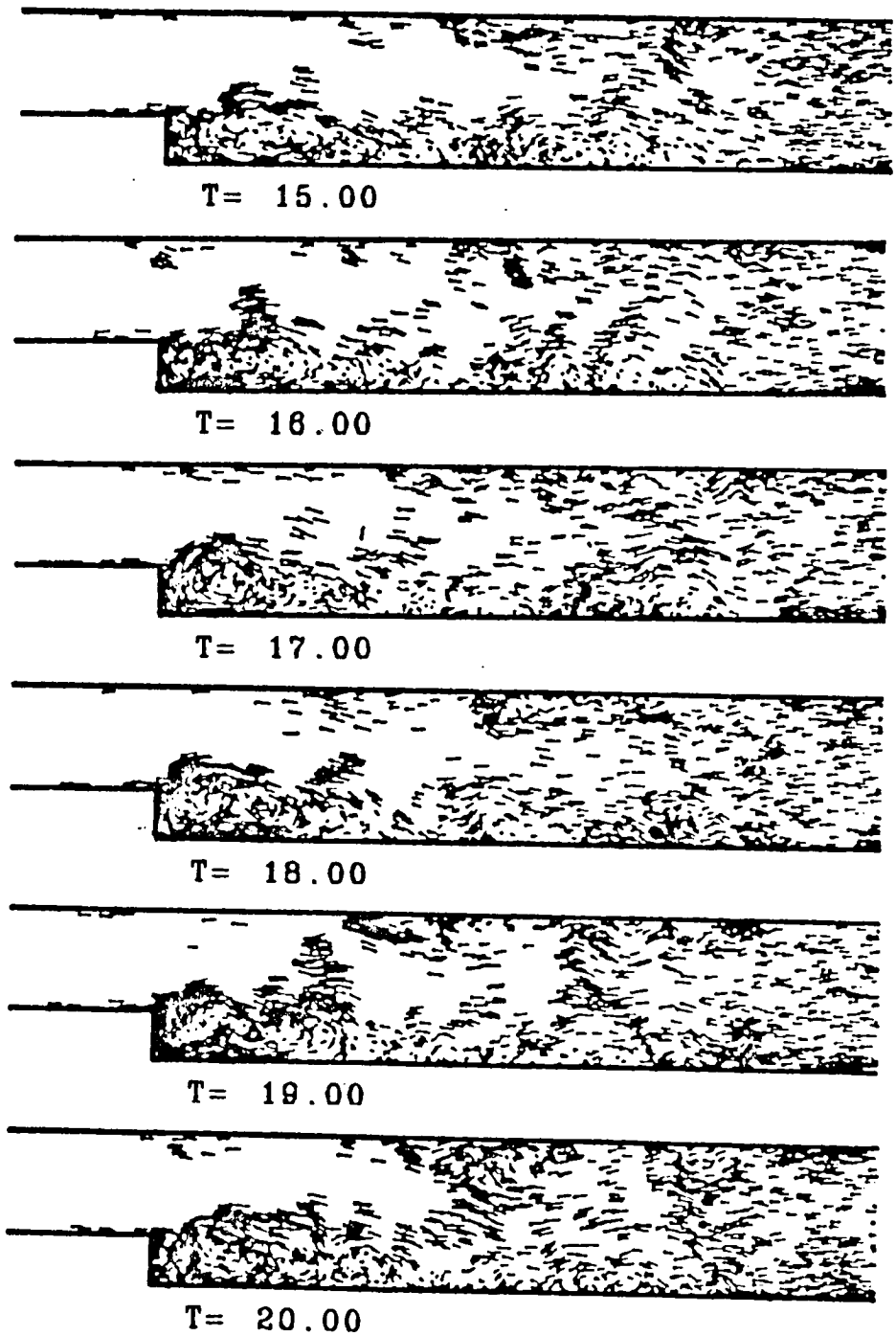

Figure 3.24. - Flow development along channel at HT = 1/3 and Re = 10^4.

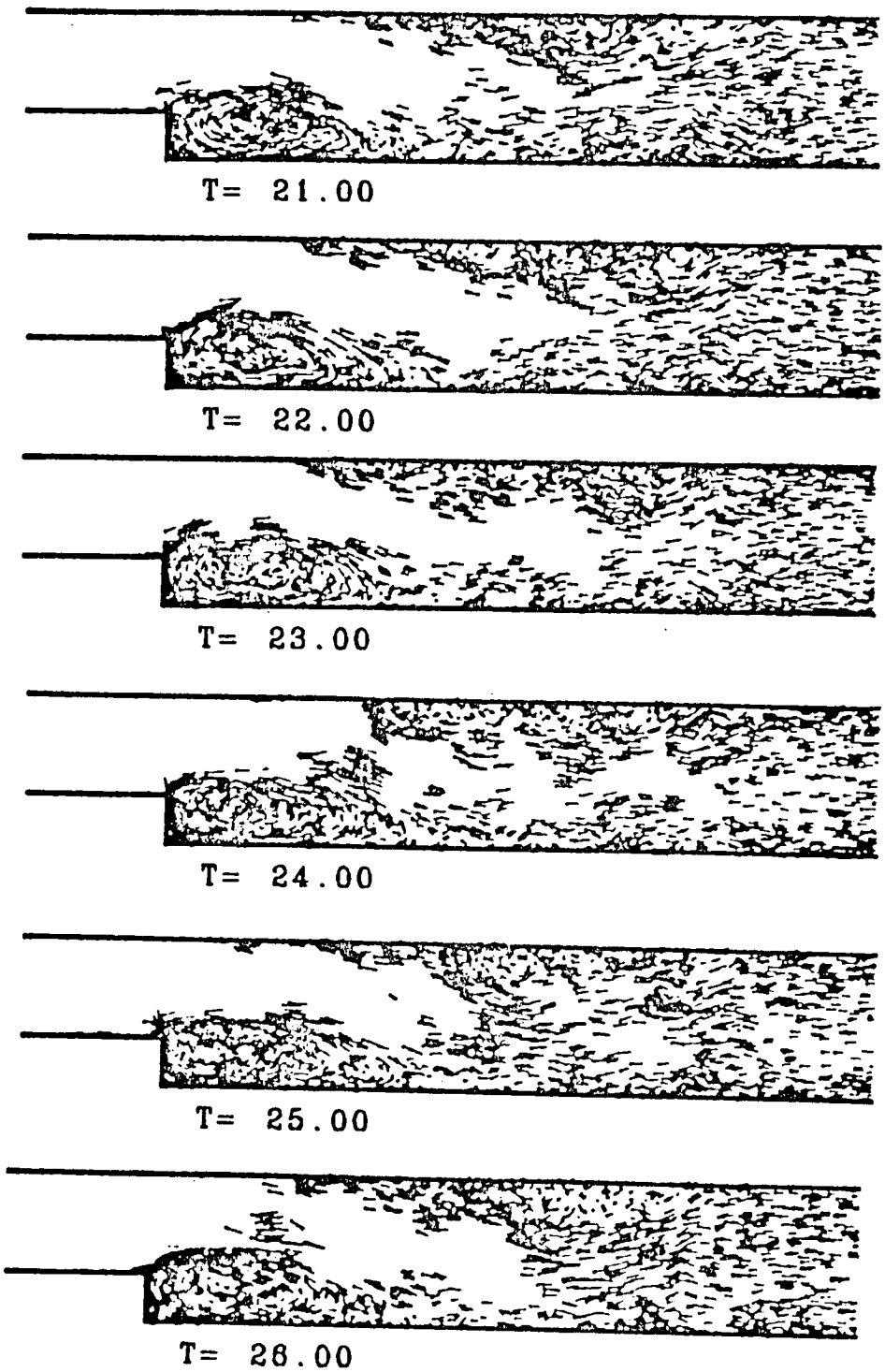

Figure 3.25. - Flow development along channel at HT = 1/3 and Re = 10^5.

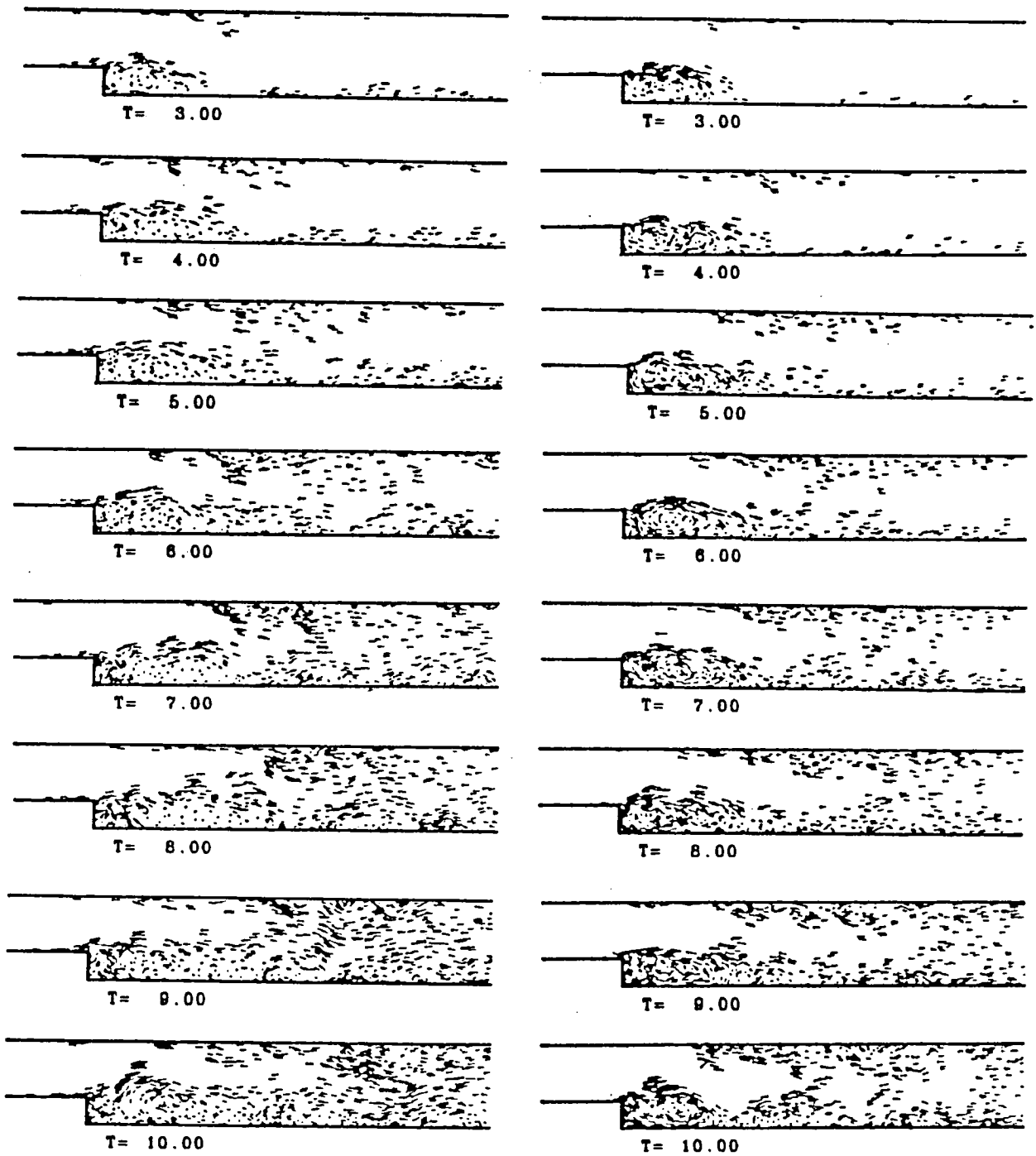

Figure 3.26. - Comparison of flow development at HT = 1/3 with different Reynolds numbers.

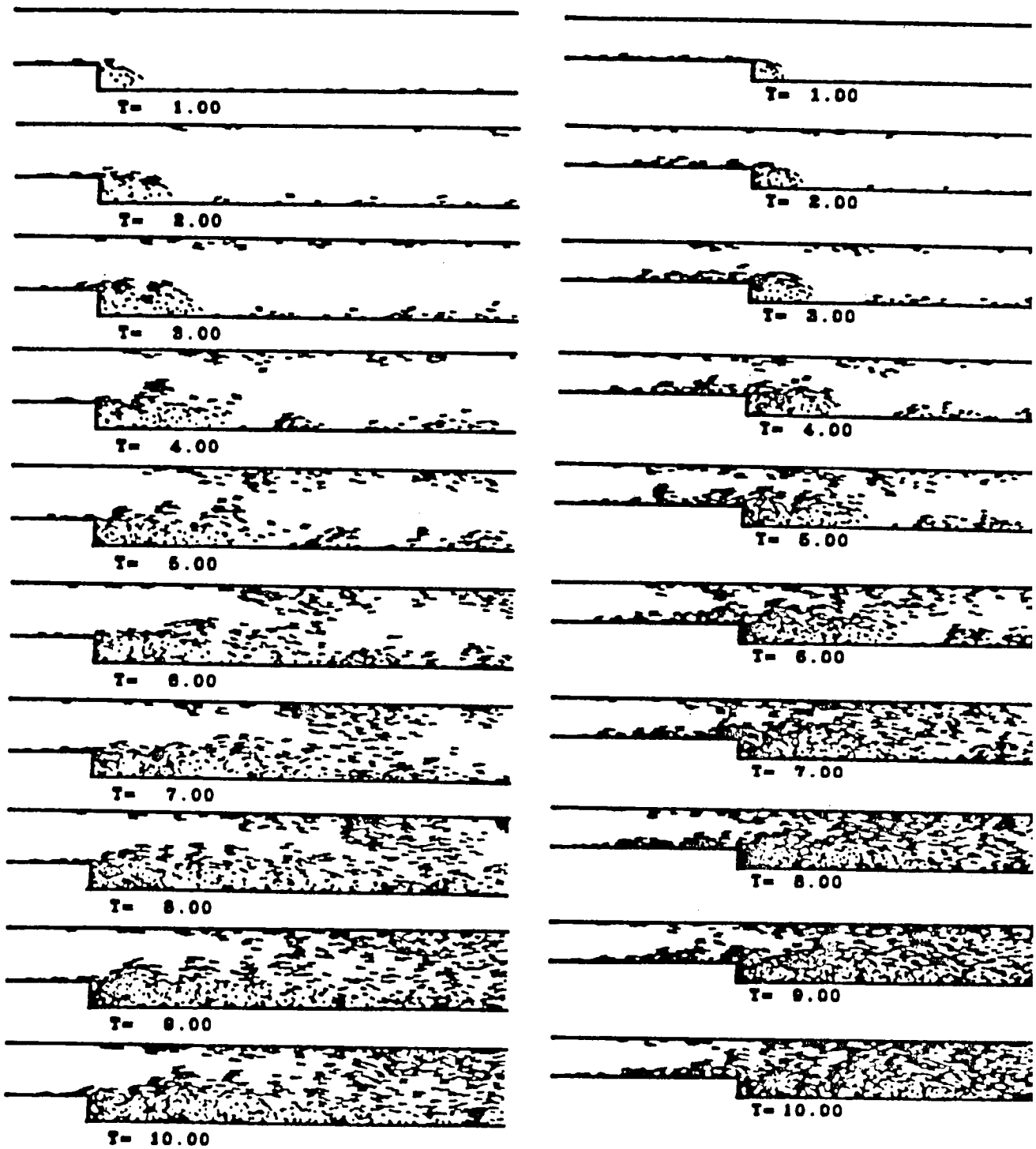

Figure 3.27. - Comparison of flow development with different inlet lengths for HT = 1/3, Re = 10^4, x_{in}(left) = 1.0, and x_{in}(right) = 3.0.

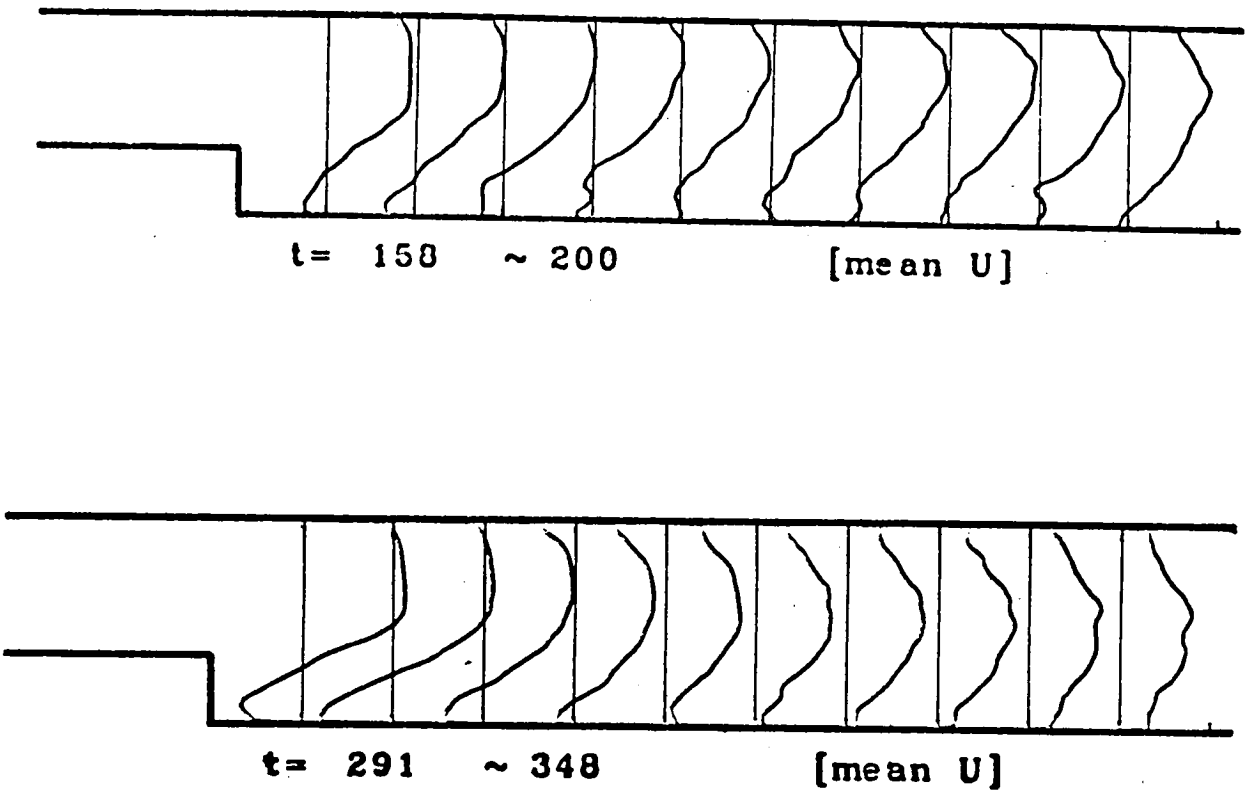

Figure 3.28. - Comparison of mean velocity profile at HT = 1/3 and Re = 10^4 with different averaging time period.

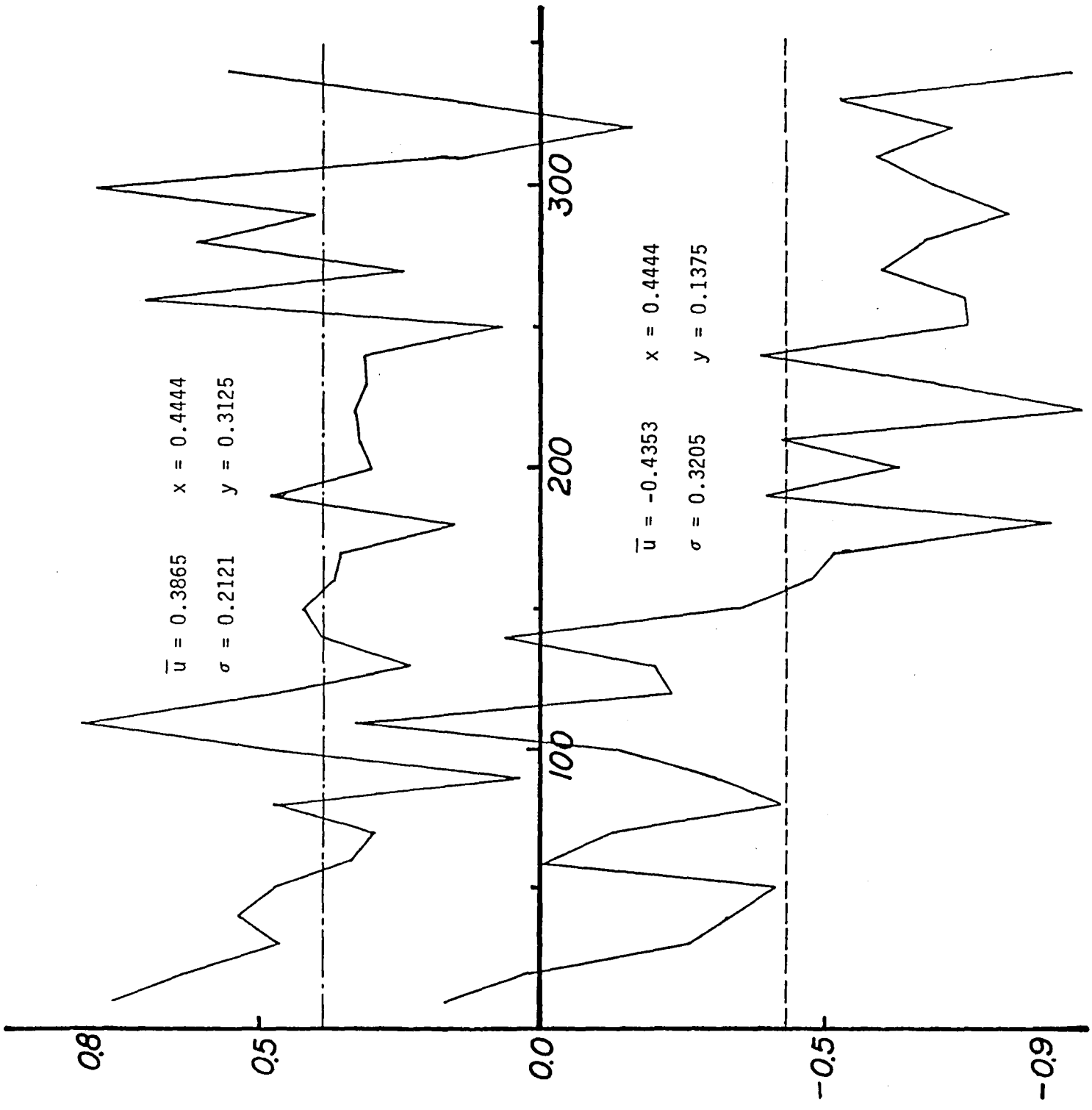

Figure 3.29(a). - Variation of streamwise velocity with time at X = 0.4444.

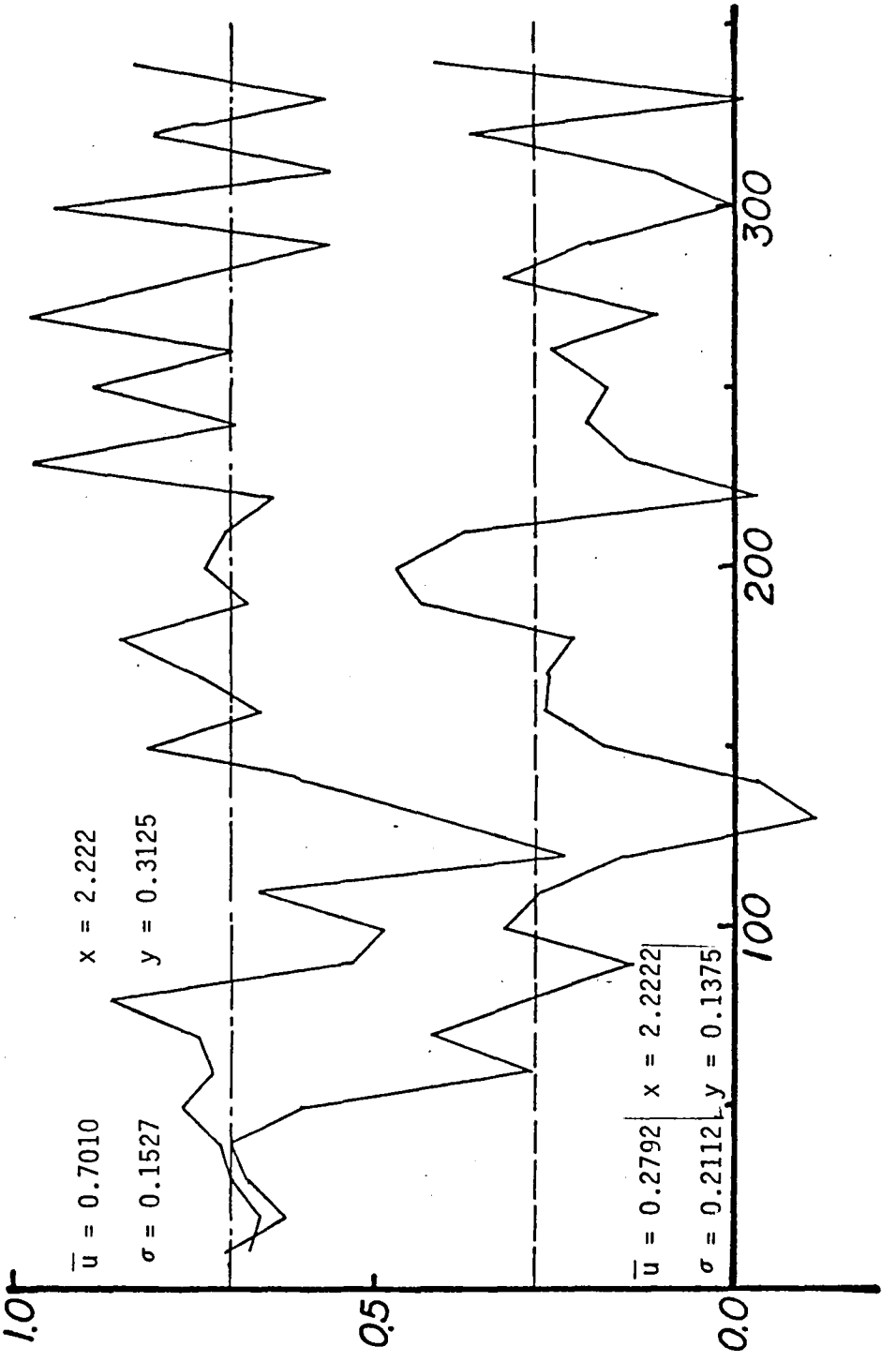

Figure 3.29(b). - Variation of streamwise velocity with time at X = 2.2222.

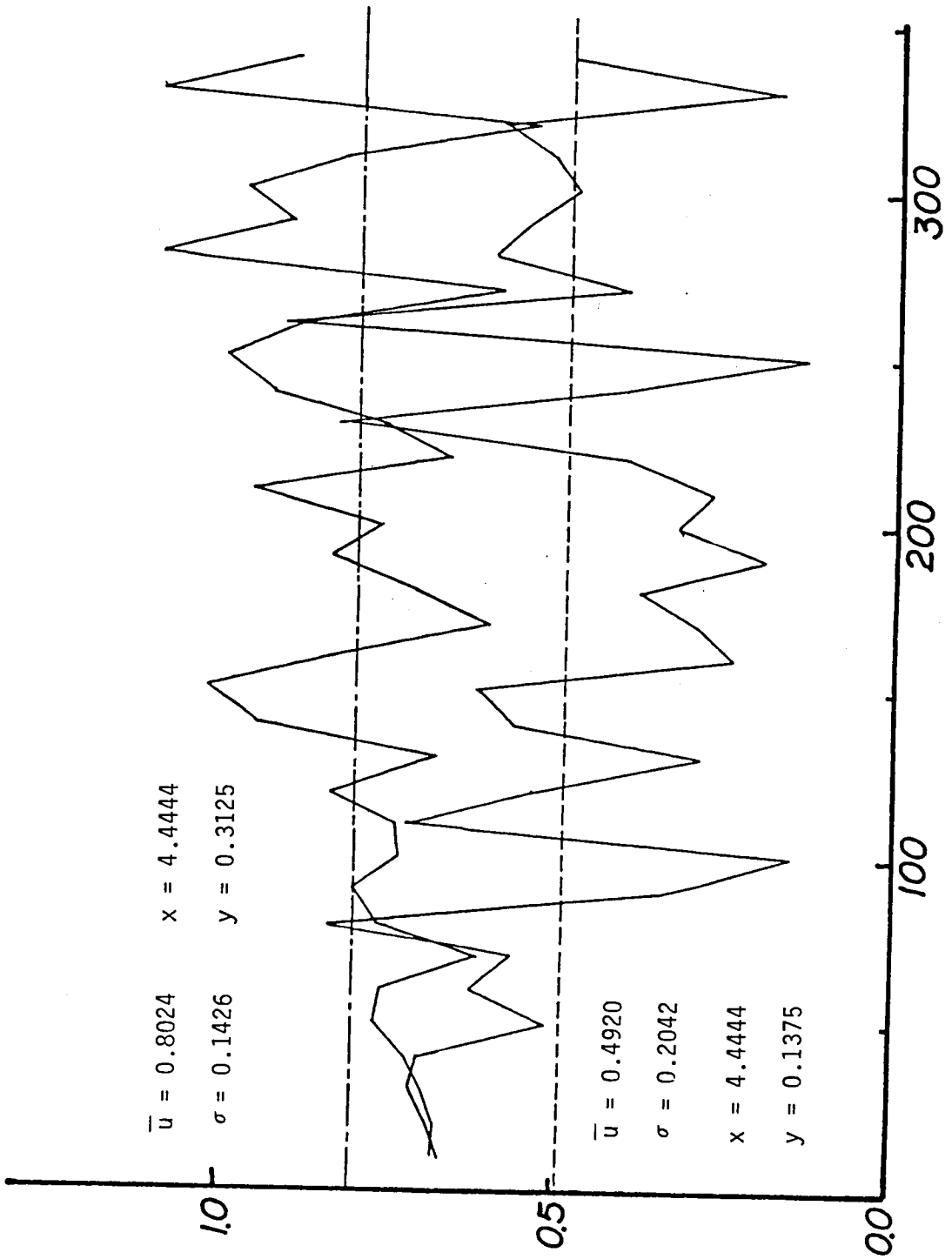

Figure 3.29(c). - Variation of streamwise velocity with time at X = 4.4444.

1. Report No.	2. Government Accession No.	3. Recipient's Catalog No.
NASA CR-168278		

4. Title and Subtitle	5. Report Date
Numerical Modeling of Turbulent Flow in a Channel	March 1983
	6. Performing Organization Code 505-31-42

7. Author(s)	8. Performing Organization Report No.
Y.-W. Dai, A. F. Ghoniem, F. S. Sherman, and A. K. Oppenheim	
	10. Work Unit No.

9. Performing Organization Name and Address	11. Contract or Grant No.
University of California Berkeley, California	NAG 3-131
	13. Type of Report and Period Covered Contractor Report

12. Sponsoring Agency Name and Address	14. Sponsoring Agency Code Report No.
U.S. Department of Energy, Office of Basic Engineering Research, Washington, D.C., and National Science Foundation	DOE/NASA/0131-2

15. Supplementary Notes

Final Report. Project Manager, C. J. Marek, Aerothermodynamics and Fuels Division, NASA Lewis Research Center, Cleveland, Ohio 44135.

16. Abstract

Two-dimensional incompressible turbulent flow in a channel with a backward-facing step was studied numerically by Chorin's Random Vortex Method (RVM), an algorithm capable of tracing the action of elementary turbulent eddies and their cumulative effects without imposing any restrictions upon their motions. The step occurs in one side of a channel with otherwise flat, parallel walls; its height equals 1/3, 1/4, or 1/5 the width of the channel downstream. The main objective was to investigate the behavior of the large-scale turbulent eddies in a flow and the flow characteristics in the separated shear layer, the reattached zone, and the rebuilding boundary layer after reattachment. The unsteady vorticity field and the distribution of time-averaged turbulent statistics were obtained. The effects of expansion step height and initial boundary layer state were also studied. Comparisons were made with the available experimental results. The agreement is satisfactory in the velocity profiles and in the reattachment length, and fairly good in the turbulence profiles. Also, a mechanism of the development of the reattaching turbulent flow was suggested by the numerical results.

17. Key Words (Suggested by Author(s))	18. Distribution Statement
Turbulence Vorticity Rearward step	Unclassified - unlimited STAR Category 07

19. Security Classif. (of this report)	20. Security Classif. (of this page)	21. No. of pages	22. Price*
Unclassified	Unclassified	68	A04

*For sale by the National Technical Information Service, Springfield, Virginia 22161